USE OF HIGH-STRENGTH STEEL REINFORCEMENT IN SHEAR FRICTION APPLICATIONS

by

Gabriel Augusto Zeno

B.S. in Civil Engineering, University of Puerto Rico at Mayagüez, 2005

Submitted to the Graduate Faculty of

Swanson School of Engineering in partial fulfillment

of the requirements for the degree of

Master of Science

University of Pittsburgh

2009

UNIVERSITY OF PITTSBURGH

SWANSON SCHOOL OF ENGINEERING

This thesis was presented

by

Gabriel Augusto Zeno

It was defended on

October 21, 2009

and approved by

Dr. John Brigham, Assistant Professor, Civil and Environmental Engineering

Dr. Julie Vandenbossche, Assistant Professor, Civil and Environmental Engineering

Thesis Advisor:

Dr. Kent A. Harries, Associate Professor, Civil and Environmental Engineering

USE OF HIGH-STRENGTH STEEL REINFORCEMENT

IN SHEAR FRICTION APPLICATIONS

Gabriel Augusto Zeno, M.S.

University of Pittsburgh, 2009

This thesis reports the results of a study associated with Task 8.4b of the National Cooperative Highway Research Program (NCHRP) Project 12-77 *Structural Concrete Design with High-Strength Steel Reinforcement*. The objective of the study is to evaluate the effects of the use of high-strength steel reinforcement in shear friction applications. Shear friction is the mechanism present when shear is transferred across an interface between two concrete members that can slip relative to one another. It arises from the roughness of the interface and the clamping force created by the steel reinforcement across it.

The study was accomplished by testing typical push-off specimens with a cold joint test interface, which had a surface roughness with at least ¼-inch amplitude in order to simulate the connection between a composite slab and an AASHTO girder. The parameters measured during the tests were the magnitude of the shear load, the shear displacement or "slip" parallel to the test interface, the crack width perpendicular to the test interface, and the strain in the steel reinforcement across the test interface.

The test results showed that the shear friction mechanism occurs in stages and that the concrete component contributes to the majority of the shear friction capacity; the steel component develops only after significant cracking. In other words, the concrete and steel components of the shear friction mechanism do not act simultaneously as implied by current design standards. In addition, the test results showed that, contrary to the assumptions of the

AASHTO and ACI equations to calculate the shear friction capacity of concrete members, the interface steel reinforcement never reaches its yield strain. Therefore, the use of high-strength reinforcing steel does not affect the shear friction capacity of concrete members because the clamping force that is part of the shear friction mechanism is a function of the elastic modulus of the steel rather than its yield strength. Based on these findings and using the experimental data from current and previous tests an alternative equation is proposed for the calculation of the shear friction capacity of reinforced concrete members.

TABLE OF CONTENTS

LIST OF TABLES

LIST OF FIGURES

PREFACE

This thesis reports the results of a study associated with Task 8.4b of the National Cooperative Highway Research Program (NCHRP) Project 12-77 *Structural Concrete Design with High-Strength Steel Reinforcement*. The objective of the present study is to evaluate the effects of the use of high-strength steel reinforcement in shear friction applications. Based on the findings of the study and using the experimental data from current and previous tests an alternative equation is proposed for the calculation of the shear friction capacity of reinforced concrete members.

ACRONYMS

AASHTO	American Association of State Highway and Transportation Officials
ACI	American Concrete Institute
LRFD	Load and Resistance Factor Design
LVDT	Linear variable displacement transducer
NCHRP	National Cooperative Highway Research Program

NOMENCLATURE

Δ	shear interface displacement or slip
ε_s	shear interface steel reinforcement strain
μ	friction factor/coefficient of friction
τ_{crack}	cracking shear stress
τ_u	ultimate shear stress
A_{cv}	shear interface concrete area
A_{vf}	shear interface steel reinforcement area
c	cohesion factor
E_s	steel reinforcement elastic modulus
f'_c	concrete compressive strength
f_y	steel reinforcement yield strength
V	applied shear load
V_{crack}	cracking shear load
V_{ni}	shear friction capacity
V_u	ultimate shear load
w	shear interface crack width

This thesis was completed using US units throughout except where noted. The following "hard" conversion factors were used:

1 inch = 25.4 mm

1 kip = 4.448 kN

1 ksi = 6.895 MPa

Reinforcing bar sizes are given using the designation cited in the appropriate reference. In the thesis, a bar designated with a "#" followed by a number refers to a standard inch-pound designation used in the United States (e.g.: #7). The number refers to the diameter of the bar in eights of an inch. A bar designated with an "M" after the number refers to the standard metric designation. The number refers to the nominal bar diameter in millimeters (e.g.: 20M).

1.0 INTRODUCTION AND LITERATURE REVIEW

For many years the design of reinforced concrete structures in the United States was dominated by the use of steel reinforcement with yield strength, f_y, equal to 40 ksi (275 MPa) and since about 1970, 60 ksi (414 MPa). Design with steel having higher yield strength values has been permitted, but since the 1971 edition of ACI 318, yield strength values have been limited to 80 ksi (552 MPa) (Lepage et al. 2008). Currently, ACI 318-08 permits the design using steel reinforcement with a yield strength defined as the stress corresponding to a strain of 0.0035, but not to exceed 80 ksi (552 MPa). The exception is transverse reinforcement where the use of yield strength up to 100 ksi (690 MPa) is permitted, but may only be applied to the requirements for confinement in compression members and not to requirements for shear, torsion, flexure or axial strength. AASHTO LRFD Specifications (AASHTO 2007) similarly limit the use of reinforcing yield strength in design to no less than 60 ksi (414 MPa) and no greater than 75 ksi (517 MPa) (exceptions are permitted with owner approval). Both ACI and AASHTO limits have been written and interpreted not to exclude the use of higher strength grades of steel, but only to limit the value of yield strength that may be used in design.

The limits on yield strength are primarily related to the prescribed limit on compressive strain of 0.003 for concrete and to the control of crack widths at service loads. Crack width is a function of steel strain and consequently steel stress (Nawy 1968). Therefore, the stress in the steel reinforcement will always need to be limited to some extent to prevent cracking from

affecting serviceability of the structure. However with recent improvements to the properties of concrete, such as the development of higher capacity concretes, the ACI 318-08 limit of 80 ksi (552 MPa) and AASHTO limit of 75 ksi (517 MPa) on the steel reinforcement yield strength are believed to be unnecessarily conservative for new designs. Additionally, an argument can be made that if a higher strength reinforcing steel is used but not fully accounted for in design, there may be an inherent over strength in the member that has not been properly accounted for. This concern is most critical in seismic applications or when considering progressive collapse states. Neither are generally significant concerns for bridge structures. The argument most often made for adopting higher reinforcing bar design stress limits is simply that it permits a more efficient use of high strength steel.

Steel reinforcement with yield strength exceeding 80 ksi (552 MPa) is commercially available in the United States (Lepage et al. 2008). If allowed, using steel with this capacity would provide various benefits to the concrete construction industry by reducing member cross sections and reinforcement quantities, which would lead to savings in material, shipping, and placement costs. Reducing reinforcement quantities would also prevent congestion problems leading to better quality of construction. Finally, coupling high-strength steel reinforcement with high performance concrete should result in a much more efficient use of both materials.

Additionally, much of the interest in higher strength steels stems from the fact that many of the higher strength grades are more resistant to corrosion and therefore very attractive in reinforced concrete applications. For instance, the ASTM A1035 reinforcing steel used in this study (commercially referred to as MMFX steel) has a yield capacity on the order of 120 ksi (827 MPa) and is reported to be between 2 and 10 times more resistant to corrosion than conventional ASTM A615 ‘black’ reinforcing steel (Shahrooz et al. 2009). In some applications,

ASTM A1035 reinforcing steel has replaced ASTM A615 steel on a one-to-one basis on the premise that it is more resistant to corrosion but not as costly as stainless steel grades (Shahrooz et al. 2009). Clearly, if the enhanced strength of ASTM A1035 steel could be used in design calculations, less steel would be required resulting in a more efficient and economical structural system.

The objective of this literature review is to discuss some of the research and experimental work done related to the use of high-strength steel for the design of reinforced concrete structures. The main findings from the research work will be summarized in order to provide an overall picture of the differences in performance between regular steel and high-strength steel on reinforced concrete structures. This literature review will focus on the changes in flexure and shear capacity, including shear friction, introduced by the change in reinforcement strength.

1.1 HIGH-STRENGTH STEEL

1.1.1 Properties

A number of high-strength steels are currently available for the design and construction of reinforced concrete flexural members (Mast et al. 2008). Figure 1.1.a shows the typical stress-strain relationships of various high-strength reinforcing steels along with the stress-strain relationship of conventional Grade 60 (414 MPa) steel for comparison. From the figure it can be seen that the stress-strain curve of typical high-strength steel is characterized by an initial linear portion followed by a nonlinear section. Significantly, there is an absence of a distinct yield plateau in most high-strength steels. Despite the lack of a well-defined yield point, most high-

strength reinforcing steels are capable of achieving ultimate strain values of 0.05 or higher (Mast et al. 2008).

1.1.2 High-Strength Steel as Flexural Reinforcement

To apply the higher resistance factor, φ, of 0.9 allowed by ACI 318-08 in the design of tension-controlled reinforced concrete flexural members, a member should exhibit a desirable ductile behavior. A desirable behavior implies that at service load, the member should display small deflections and minimal cracking; at higher loads the member should display large deflections and sufficient cracking to provide warning before reaching its nominal capacity. Both deflection and cracking are primarily a function of steel strain near the tension face of the member, and in general, desirable behavior of a member is related to ductility, which relates to yielding or inelastic deformation of the steel reinforcement. For lower strength reinforcing materials, the only way to obtain high strains near the tension face at nominal strength is to ensure yielding of the tension steel, however, for high-strength materials, this is no longer necessary (Mast, et al. 2008).

The objective of the work reported by Mast et al. (2008), was to assess the adequacy of a proposed 100 ksi (690 MPa) reinforcement stress-strain relationship for Microcomposite Multistructural Formable (MMFX) steel in order to establish acceptable strain limits for tension-controlled and compression-controlled sections reinforced with this high-strength steel. This MMFX steel is described by the ASTM A1035 specification. Mast et al. studied the behavior of concrete beams at service level and nominal strength, and determined the section behavior using a cracked section analysis that satisfied equilibrium and compatibility. They assumed an elastic stress distribution under service load and used the ACI rectangular stress block at nominal

capacity. However, between these two limits, they used a trapezoidal stress block for concrete consisting of an initial linear portion with an elastic modulus $E_c = 57000\sqrt{f'_c}$ psi ($4730\sqrt{f'_c}$ MPa), up to a stress of $0.85f'_c$ followed by a plastic plateau.

Figure 1.1.b shows the reinforcement stress-strain relationship model developed by Mast et al. (2008) for MMFX steel. The model, which is a simplification of the empirically derived stress-strain relationship given by Equation 1.1, is represented by an initial linear-elastic portion with an elastic modulus E_s = 29,000 ksi (200,000 MPa), followed by a perfectly plastic yield plateau with a yield strength of 100 ksi (690 MPa). The simplified elastic-plastic model is essentially equivalent to increasing the current ACI 318 limit on the steel reinforcement yield strength, f_y, from 80 ksi (550 MPa) to 100 ksi (690 MPa).

$$f_s = \begin{cases} 29{,}000\epsilon_s & \epsilon_s \le 0.00241 \\ 170 - \dfrac{0.345}{\epsilon_s + 0.00104} & 0.00241 < \epsilon_s < 0.060 \end{cases} \text{ (ksi)} \qquad \text{(Eq. 1.1.a)}$$

$$f_s = \begin{cases} 200{,}000\epsilon_s & \epsilon_s \le 0.00241 \\ 1172 - \dfrac{2.379}{\epsilon_s + 0.00104} & 0.00241 < \epsilon_s < 0.060 \end{cases} \text{ (MPa)} \qquad \text{(Eq. 1.1.b)}$$

For the nominal strength, Mast et al. (2008) performed a numerical analysis considering a rectangular, singly reinforced concrete section having a number of different reinforcement ratios. They considered a concrete compressive strength, f'_c, of 6500 psi (45 MPa) with an ultimate strain, ε_{cu}, of 0.003 at the extreme compression face of the concrete. The three different reinforcement stress-strain relationships used were the actual behavior of the reinforcing steel, as defined by Equation 1.1, the elastic-plastic simplification having the ACI 318-08 limit of 80 ksi (552 MPa), and the proposed 100 ksi (690 MPa) limit. In addition, they considered the stress-strain relationship of conventional Grade 60 (414 MPa) reinforcement for comparison purposes.

Mast et al. (2008) calculated the balanced reinforcement ratios, ρ_b, as 3.95%, 2.60%, and 1.85% for the sections using the Grade 60 (414 MPa), 80 ksi (552 MPa), and 100 ksi (690 MPa) reinforcement grades, respectively. The results are shown in Figure 1.1.c. From the figure it can be inferred that for a reinforcement ratio greater than 3.95%, the calculated nominal moment capacity of the section was equal for all of the different models because the section behavior was controlled by concrete compression; i.e.: failure was governed by crushing of the concrete prior to yielding of the reinforcing steel. For sections with a reinforcement ratio less than 1.75% (typical value for reinforced concrete beams), the use of the 100 ksi (690 MPa) elastic-plastic model typically underestimated the nominal moment capacity of the section with respect to the actual behavior. On the other hand, for reinforcement ratios between 1.75 and 2.7%, the use of the 100 ksi (690 MPa) limitation slightly overestimated the capacity of the section. However, this difference was on the order of 2.5%, which was considered insignificant for design purposes.

To investigate the adequacy of the various reinforcement stress-strain relationships, Mast et al. (2008) calculated the nominal moment capacity, M_n, of an arbitrary beam having a width, b, equal to 12 in. (305 mm), an effective depth, d, equal to 24 in. (610 mm), and a reinforcement ratio, ρ_b, equal to 1%. The calculated nominal moment capacities of the sections are given in Table 1.1 for the three different high-strength reinforcement stress-strain relationship models and also for conventional Grade 60 (400 MPa) reinforcement. From the table it can be seen that the design using the proposed simplified model results in more efficient use of the high-strength characteristics when compared to the design using the 80 ksi (552 MPa) limit because it provides results that are closer to the actual capacity of the section while still providing a significant reserve capacity.

In order to establish suitable design limits for tension-controlled and compression-controlled sections with high-strength steel reinforcement Mast et al. (2008) performed moment-curvature and moment-deflection analyses based on current design practice. The results from the moment-curvature analysis are shown in Table 1.2. The moment-curvature analyses were performed for a beam reinforced with high-strength steel at the tension-controlled strain limit of 0.0066 and a concrete strength, f'_c, of 5000 psi (34 MPa). Equation 1.1 was used to represent the stress-strain relationship of the reinforcing steel. From Table 1.2 it can be seen that the deflection ratio, δ (ratio between the deflections at nominal strength and service load), was greater for the higher strength steel than for the conventional steel; this needs to be accounted for by appropriately designing the depth of the member. In addition, due to the higher tension strain in the high-strength reinforcement under service loading conditions, the beams may exhibit larger crack widths than if reinforced with conventional steel. However, as shown in Mast et al. (2008), previous testing indicates that the measured crack width under service loading conditions is only slightly larger than the (so-called) acceptable crack widths for beams reinforced with conventional steel. It is proposed that since some high-strength steels like MMFX have improved corrosion resistance, the increased crack widths could be acceptable as long as these are not aesthetically objectionable.

Based on the stress-strain relationship model for MMFX steel (Figure 1.1.b) and the current limitations for acceptable behavior, Mast et al. (2008) proposed the variation of the flexural resistance factor, φ, shown in Figure 1.1.d to be used when the steel reinforcement yield strength, f_y, is taken as 100 ksi (690 MPa). To help prevent compression-controlled failure, they suggest providing high-strength or conventional compression reinforcement; however, if high-strength compression steel is used, the ACI 318-08 design yield strength limit of 80 ksi (550

MPa) should be maintained for the compression reinforcement. This limit is based on the maximum stress that can be developed at a strain of 0.003, which is the ultimate concrete strain at the extreme compression face of the concrete beam.

As demonstrated by Mast et al. (2008), flexural members designed using the simplified design method and the criteria mentioned above will have flexural strength characteristics comparable to members designed according to current ACI 318-08 requirements using conventional Grade 60 (414 MPa) or Grade 75 (522 MPa) reinforcing steel.

1.1.3 High-Strength Steel as Shear Reinforcement

The shear behavior of conventionally-reinforced concrete beams is not well understood and in current design codes, including ACI 318-08, calculation of the shear strength is based on semi-empirical relationships. Therefore, the calculated shear strength can vary significantly (up to 250 %) among the different code approaches (Hassan, et al. 2008). Similarly, the behavior of concrete members reinforced with high-strength steel and subjected to shear is not well defined. One concern is whether the high stress levels induced in the reinforcement may cause excessive cracking in the concrete resulting in degradation of the concrete component of shear resistance. Another concern is how accurately the current design codes can predict the shear strength of concrete members reinforced with high-strength steel (Sumpter 2007).

The objective of the work reported by Sumpter (2007) was to determine the feasibility of using high-strength steel as shear reinforcement for concrete members, particularly focusing on the member behavior under overload conditions with the steel being at high stress levels. The specimens used in the experimental program were nine reinforced concrete beams divided into three main categories according to the combination of flexural and shear reinforcement steel

used, which were conventional ASTM A615 Grade 60 steel and ASTM A1035 steel. For each category, the stirrup spacing varied to reflect a minimum, intermediate, and maximum level of shear reinforcement as allowed by ACI 318-05, (current version at the time of the experiments). All the beams had cross-sectional dimensions of 16 x 12 in. (406 x 305 mm), and a total length of 16 ft (4.88 m). In addition, all beams were provided the same longitudinal reinforcement ratio in order to be able to attribute changes in the observed behavior to either the high-strength steel or the stirrup spacing. All shear steel reinforcement consisted of #3 (9.5 mm) stirrups.

The specimen test matrix used by Sumpter (2007) is shown in Table 1.3. It labels beams using three parameters: type of longitudinal steel, type of transverse steel, and the spacing of the transverse steel in inches. The letter "C" indicates conventional Grade 60 steel while the letter "M" indicates MMFX steel. The nine beams were subjected to a load that increased at approximately 15 kip (66.7 kN) increments until failure. The ultimate shear load for each beam, V_{exp}, is also shown in Table 1.3.

In terms of the shear load versus deflection relationship, the experimental results showed that the maximum measured deflections were approximately equal to 0.7 in. (17.8 mm). These relatively small deflections were attributed to the primarily shear mode of failure. The experimental results also indicated that the stiffness of each beam set was almost identical regardless of the type of reinforcement. In general, it was found that increasing the transverse reinforcement ratio, by reducing the stirrup spacing, increases both the load-carrying capacity and deflection at failure. However, using different types of longitudinal and transverse steel within a given beam set, only affects the ultimate load-carrying capacity. These results are shown in Figure 1.2.a.

The experimental results also showed that for the C-C (conventional longitudinal and shear reinforcement) specimens, the behavior in terms of the shear load versus transverse strain relationship was linear until yielding of the stirrups and then became nonlinear. In this case, failure of the specimen occurred right after yielding of the longitudinal reinforcing bars. On the other hand, for the C-M (conventional longitudinal and MMFX shear reinforcement) specimens the behavior was linear until yielding of the stirrups but then appeared to plateau. This was attributed to the higher yield strain and strength of MMFX steel in comparison to Grade 60 steel. The behavior of the M-M (MMFX longitudinal and shear reinforcement) specimens was similar to the behavior of the C-M specimens. However, the M-M specimens were better at controlling the crack width at a given load level in comparison to the other two. The high level of strain induced in the transverse and longitudinal steel for the M-M specimens allowed the compression strain in the diagonal direction to reach its ultimate value, which caused crushing of the concrete. This mechanism was demonstrated by the nonlinear behavior before failure, which is shown in Figure 1.2.b. From these results it was concluded that failure was mainly due to the concrete and did not fully utilize the strength of high-strength steel shear reinforcement beyond about 80 ksi (552 MPa).

The results for the shear load-crack width relationships showed that all shear crack width values at service loads were less than the ACI implied limit for flexural cracking of 0.016 in. (0.41 mm), regardless of the setup type or beam type. These results are shown in Figure 1.2.c. The two beam types containing high-strength steel stirrups showed smaller shear crack widths at the service load level in comparison with the beams reinforced with conventional steel, which suggests that direct (one-to-one) replacement of conventional steel with MMFX steel reduces the shear crack width at service load levels. The improved behavior at the serviceability condition

was attributed by Sumpter to the enhanced bond characteristics of ASTM A1035 steel (including MMFX) due to its rib configuration. The cracking pattern at each load level was almost the same for all three beams of a given set. However, beams reinforced entirely with high-strength longitudinal and transverse steel typically had a larger number of small cracks dispersed along the span length than the other beams. This was also attributed to the capability of ASTM A1035 steel to distribute cracks and control crack width in comparison with conventional Grade 60 reinforcement due to the enhanced rib configuration. These conclusions are interesting because there is typically no difference between the rib configuration of ASTM A615 and A1035 reinforcing steels and Sumpter does not report a difference in his test program.

1.2 SHEAR FRICTION

1.2.1 Mechanisms of Shear Friction

The shear-carrying mechanism present when shear is transferred across an interface between two members that can slip relative to one another is commonly known as aggregate interlock, interface shear transfer, or shear friction. The last of these terms will be used here. The interface on which the shear acts is referred as the shear or slip plane. Schematic representations of the shear friction mechanism are shown in Figure 1.3.

The shear friction mechanism arises from the roughness of the concrete interfaces. From Figure 1.3.a it can be seen that, as a rough interface displaces or slips in a shear mode resulting in a deformation, Δ, a wedging action develops, forcing the crack width, w, to increase in the direction perpendicular to the interface. This opening or dilation of the shear crack engages the

reinforcement crossing the crack resulting in a clamping force, $A_{vf}f_y$, being generated. Shear friction is an analogy used in design to represent a mechanism that is considerably more complex than conventional friction. The mechanism certainly includes the effect of friction, but also other phenomena that will be discussed in Section 1.2.2.

The "coefficient of friction" from ACI or "friction factor" from AASHTO, μ, is actually a measure of the surface roughness as idealized by a sawtooth shear interface having an angle, φ, as described by Birkeland and Birkeland (1966), and shown in Figure 1.3.a. From equilibrium conditions, the equation for shear friction proposed by Birkeland and Birkeland in 1966 is:

$$V_{ni} = A_{vf} f_y \tan \varnothing \qquad \text{where:} \qquad \tan \varnothing = \begin{cases} 1.7 \text{ for monolitic concrete} \\ 1.4 \text{ for artificially roughened joints} \\ 1.0 \text{ for ordinary joints} \end{cases} \qquad \text{(Eq. 1.2)}$$

In this equation:

V_{ni} = Nominal shear friction capacity

A_{vf} = Interface steel reinforcement area

f_y = Interface steel reinforcement yield strength

φ = Angle of idealized sawtooth shear interface

The understanding of the shear friction resisting mechanism has evolved to recognize the complex nature of the crack interface behavior as shown in Figure 1.3.b and to include the aggregate and cement matrix properties, dowel action and localized effects of reinforcement within the interfacial area as shown in Figure 1.3.c. Walraven and Reinhardt (1981) provided a remarkably detailed description of the components of interface behavior. Regardless of increasing complexity in terms of understanding, code-based provisions for shear friction have maintained the simple format proposed by Birkeland and Birkeland (1966). In fact, ACI

provisions continue to maintain the upper limit on interface shear of 800 psi (5.5 MPa) proposed by Birkeland and Birkeland.

The clamping force attributed to the interface reinforcing steel is engaged as the crack opens, thus the clamping force is passive in nature. The crack must open sufficiently to develop the design clamping force, $A_{vf}f_y$. Loov and Patnaik (1994) concluded that a shear displacement, Δ, of 0.02 in. (0.5 mm) is required to yield conventional mild reinforcing steel having a yield strength, f_y, of 60 ksi (414 MPa). They additionally pointed out the inconsistency of limiting the shear displacement to a lower value since this is insufficient to generate yield in the interface steel reinforcement (a previous proposal by Hanson (1960) limited the shear displacement to 0.005 in. (0.13 mm)). Most critical to this discussion is the fact that there is limited data available for mild interface steel reinforcement having nominal yield strength greater than 60 ksi. Kahn and Mitchell (2002) reported a case where the actual yield strength of the interface steel reinforcement was either 70 or 83 ksi (483 or 572 MPa). In this study, they reported significantly increased scatter in shear friction prediction reliability when using the actual yield strength values and concluded that it should not be taken to exceed 60 ksi (414 MPa) for design. In addition, when normalized by concrete strength, their experimental results showed no effect resulting from the different yield strength values as can be seen in Figure 1.4. On the contrary, from Figure 1.4 it can also be seen that Hofbeck et al. (1969) reported a modest effect as the yield strength of the interface steel reinforcement increased from 51 to 66 ksi (352 to 455 MPa), however, the reported data in this case may simply represent the natural scatter expected in such experiments. Figure 1.4 shows interface shear stress versus interface reinforcing ratio data for a range of yield strength values. All data reported is for monolithically cast test specimens.

Any real compression force resulting from load conditions across the interface also results in clamping force. Unlike the clamping force generated by the interface reinforcement, this force is active in nature and is constant regardless of the crack opening. Walraven and Reinhardt (1981) emphasized that the fundamental shear friction behavior resulting from these two sources of clamping force (internally and externally generated) differ significantly.

In addition to the friction induced by clamping forces, a component of shear friction attributed to cohesion was proposed by Mattock (1974). This model of interface behavior characterizes the interface roughness in terms of a general and a local roughness. The clamping component of shear friction is associated with the general roughness as described previously. The cohesion term reflects the shearing off of the local asperities along the crack faces. Using this analogy, the cohesion term should be expected to degrade with increasing shear displacement along the crack interface as the local roughness is reduced.

Finally, dowel action of the interface reinforcement is shown by Walraven and Reinhardt (1981) to be relatively insignificant for slip values up to at least 0.1 in. (2.5 mm). Dowel action is not explicitly considered in shear friction calculations.

1.2.2 Crack Width, Shear Displacement and Aggregate Interlock

Based on the previous discussion, it is evident that crack width, *w*, is the critical interface behavior affecting shear friction. Crack width affects the clamping force developed in the interface reinforcing steel, and it must be sufficient to engage the yield capacity of the steel. In addition, crack width affects the cohesion component of shear friction in an adverse manner (i.e. larger crack openings lead to reduced cohesion-related forces).

Based on the kinematics of the shear friction behavior shown in Figure 1.3, crack width, w, is related to the shear displacement, Δ, and the surface roughness of the interface. Due to the kinematic nature of the Δ-w relationship, it should not be expected that the amount of clamping force will significantly affect this relationship. Walraven and Reinhardt (1981) demonstrated very little effect on the Δ-w relationship for monolithically cast concrete despite varying the interface reinforcing ratio, $\rho_v = A_{vf}/A_{cv}$, from 0.56% to 2.23% as can be seen in Figure 1.5. From Figure 1.5 it can also be seen that the concrete strength, f'_c, has some effect on the Δ-w relationship since a small increase in crack width, w, is noted as the concrete strength is increased. This observation reinforces the behavior represented in Figure 1.3.b, where the stronger concrete matrix will allow the aggregate to "slide up" over the matrix rather than "crush into" it as may be the case with the weaker matrix. Walraven and Reinhardt (1981) also showed that an increase in surface roughness resulted in an increase in crack width. In this study the variation in roughness was modest and was affected by aggregate grading in the concrete mix design for these monolithically cast specimens.

The implication of Equation 1.2 and the subsequent discussions is that shear friction, which is a function of the normal clamping force, is also a function of the Δ-w crack dilation relationship. Aggregate interlock controls the Δ-w relationship. Prior to cracking along the shear interface, clamping force resulting at the interface reinforcement is negligible. Following cracking, the passive clamping force is engaged by the Δ-w relationship, which for small values of shear displacement remains essentially linear as can be seen in Figure 1.5. On the other hand, the relationship between shear stress and shear displacement, τ-Δ, has been reported to be nonlinear from the initiation of cracking (Loov and Patnaik 1994, Walraven and Reinhardt 1981) due to the degradation of cohesive forces as the crack width increases. When the interface steel

reinforcement yields, the clamping force no longer increases and the shear friction is at best constant, or begins to degrade as the crack width continues to increase. After a certain value of shear displacement, cohesion forces are overcome and shear friction capacity drops to a residual value no longer affected by continued shear displacement (Loov and Patnaik 1994, Kahn and Mitchell 2002).

Therefore, crack width affects the available shear friction force, particularly the cohesive component. As the crack width increases, the cohesive component decreases. This may be interpreted as the loss of the contribution of smaller asperities along the crack interface as the crack width increases. Walraven and Reinhardt (1981) illustrated this effect using gap-graded concrete mixes. In the gap-graded mix, there are proportionally smaller asperities (sand aggregate, in this case). These become ineffective as the crack width increases resulting in a reduced shear capacity. The value of the friction factor, $\mu = \tau/\sigma$, is reduced at larger crack widths and for "smoother" surfaces. This effect is illustrated schematically in Figure 1.6 which is based on experimental results supplemented by analytical results reported by Walraven and Reinhardt.

1.2.3 AASHTO and ACI Shear Friction Provisions

Considering only normal weight concrete and interface reinforcement oriented perpendicular to the interface, the provisions from AASHTO LRFD (2007) and ACI 318 (2008) to calculate the nominal shear friction capacity, V_{ni}, are as follows:

AASHTO 5.8.4:

$$V_{ni} = cA_{cv} + \mu(A_{vf}f_y + P_c) \qquad \text{(Eq. 1.3)}$$

$$V_{ni} \leq K_1 f'_c A_{cv}$$

$$V_{ni} \leq K_2 A_{cv}$$

$A_{vf} \geq 0.05 A_{cv} / f_y$

$V_u \leq \mu(A_{vf} f_y + P_c)$ if using this equation to calculate required A_{vf}.

ACI 318 11.7.4:

$$V_{ni} = A_{vf} f_y \mu \quad \text{(Eq. 1.4)}$$

$V_{ni} \leq 0.20 f'_c A_{cv}$

$V_{ni} \leq 800 A_{cv}$

Recall that AASHTO uses units of ksi for all stresses while ACI uses units of psi. In the equations above:

V_{ni} = Nominal shear friction capacity

A_{cv} = Area of concrete shear interface

A_{vf} = Interface steel reinforcement area

P_c = Permanent net compressive force applied across the interface

f_y = Interface steel reinforcement yield strength ≤ 60 ksi (414 MPa) for AASHTO and ACI

f'_c = Concrete compressive strength

μ = Friction factor (AASHTO) or Coefficient of friction (ACI)

c = Cohesion factor reported to account for cohesion and aggregate interlock

K_1 = Fraction of concrete strength available to resist interface shear

K_2 = Limiting interface shear resistance

1.2.3.1 Comparison

In Equation 1.3, AASHTO introduces the term cA_{cv}, which is intended to account for the effects of cohesion and aggregate interlock at the crack interface. The inclusion of this concrete term requires a minimum interface reinforcement to also be required since V_u can potentially be less than cA_{cv}, technically requiring no reinforcement across the interface. As can be seen in

Equation 1.4, ACI does not account for these crack interface properties in the calculation of the shear friction capacity, since an unroughened condition is assumed. Therefore ACI limits are computationally more conservative than those of AASHTO. However, ACI reports in the commentary to Section 11.7.4.3, that the values of the coefficient of friction, μ, account for experimentally observed behavior, and therefore, presumably include the effects of aggregate interlock and cohesion, not accounted for directly by Equation 1.4. Thus there is an inconsistency between AASHTO and ACI on shear friction behavior.

The introduction of the cA_{cv} term in Equation 1.3 by AASHTO may be unconservative, particularly at typical values of interface reinforcement ratio ($\rho_v = A_{vf}/A_{cv} < 0.02$). The data in Figure 1.7 is shown for the case of monolithically cast concrete with a compressive strength, f'_c, of 6 ksi (41.1 MPa) and having steel reinforcement with a yield strength, f_y, of 60 ksi (414 MPa). Figure 1.7.a shows the values of shear friction capacity, V_{ni}, per square foot (i.e. $A_{cv} = 144$ in^2) calculated with the equations presented here from AASHTO, ACI, Birkeland and Birkeland (1966) (Equation 1.2 above), and Kahn and Mitchell (2002) (Equation 1.5 below). Figure 1.7.b plots the same data as an equivalent friction factor defined as: $\mu = V_{ni}/A_{vf}f_y$. While an appropriate nominal value of the friction factor, μ, is 1.7 (Birkeland and Birkeland 1966) and the design value is taken as 1.4, the equivalent value of the friction factor calculated using the AASHTO relationship when the interface reinforcement ratio is equal to 0.005 is 2.73. Moreover, the equivalent friction factor at the minimum reinforcing ratio of 0.0008 is 9.8. These friction factor values are significantly higher than the values suggested by AASHTO shown in Table 1.4. While the values change, the trends and relationships shown in Figure 1.7 remain the same for all surface conditions. If the yield strength is increased, the relationships remain the same, although the limiting values are reached at lower reinforcing ratios. The inclusion of the cA_{cv} term

increases the shear friction capacity to arguably unwarranted levels. It is noted, that for steel reinforcement with yield strength equal to 60 ksi (414 MPa), the minimum interface reinforcing ratio is 0.0008. Therefore, it can be seen that contrary to the assertions in the AASHTO commentary, the inclusion of the cA_{cv} does not help to calibrate the equation with existing experimental data. For this reason it is reiterated that the friction factor, μ, is not a coefficient of friction in the classical sense because it also accounts for the effects of aggregate interlock and cohesion.

1.2.3.2 Limitations

This discussion does not address the values of the parameters used in either the AASHTO or ACI codes, assuming that these represent the consensus of the committees drafting these documents. Nonetheless, it is noted that all parameters (μ, c, K_1 and K_2) are empirical in nature and therefore subject to the limitations implied by the dataset from which they were obtained. Two issues noted in this regard are:

1) There is no data available for interface reinforcing steel having nominal yield strength exceeding 60 ksi (414 MPa). Additionally, all data is based on mild steel and thus a yield plateau is assumed.
2) There is limited data available for higher strength concrete materials. Indeed most early recommendations, still used in present codes, are based on a limited range of concrete strengths (as noted by Walraven et al. 1987). Furthermore, the commentary to AASHTO 5.8.4.1 notes the lack of data for higher strength concrete.

Finally the nature of empirical calibration must be considered. The application of the parameters μ and c, implicitly assumes that the interface reinforcement is yielding. Most significantly, it has been shown that the phenomenon represented by the parameter c deteriorates

with increasing shear displacement. Thus the recommended values for this parameter are implicitly based on a particular limit state, one which assumes yield of the interface reinforcing steel since these are assumed to occur simultaneously at the design limit state. By this argument, introducing a substantially different reinforcing material requires a recalibration of all parameters.

1.2.4 High Strength Concrete and Reinforcing Steel

Kahn and Mitchell (2002) conducted an extensive study of shear friction in high strength concrete (up to 14 ksi (97 MPa)). They proposed an equation similar in form to the AASHTO equation (Equation 1.3) for monolithically cast concrete:

$$V_{ni} = 0.05A_{cv}f'_c + 1.4A_{vf}f_y \leq 0.2A_{cv}f'_c \qquad \text{(Eq. 1.5)}$$

In this equation:

V_{ni} = Nominal shear friction capacity

A_{cv} = Area of concrete shear interface

A_{vf} = Interface steel reinforcement area

f_y = Interface steel reinforcement yield strength $\leq$ 60 ksi (414 MPa)

f'_c = Concrete compressive strength

Despite testing interface steel reinforcement having a yield strength of 83 ksi (572 MPa), Kahn and Mitchell (2002) specifically recommend maintaining the 60 ksi (414 MPa) limit on the yield strength. Similarly, Loov and Patnaik (1994) cite work by Walraven (1991) in making their assertion that “reinforcement with higher yield strength will not increase the shear strength proportionally”. The hypothesized reason for this is that while the available clamping force may increase, it does so at the expense of larger crack widths which result in decreased contributions

from aggregate interlock and cohesion. The experimental results from Kahn and Mitchell (2002) for cold-joint pushoff specimens are shown in Table 1.5.

Table 1.1: Beam capacity for different reinforcing steel models from Mast et al. (2008).

Reinforcing steel material model	Moment capacity, kip-ft (KN-m)	Capacity Ratio	Reserve capacity, kip-ft (KN-m)
Grade 60 (414 MPa) steel	327 (443)	1.00	-
Actual behavior	639 (867)	1.95	0 (0)
Simplified 100 ksi (690 MPa) model	524 (711)	1.60	115 (156)
80 ksi (552 MPa) limitation	427 (579)	1.31	212 (288)

Table 1.2: Results of moment-curvature analysis from Mast et al. (2008).

ACI 318 Code	Criterion	Steel type	Area of steel, in.^{2} (mm^2)	Steel stress at service, ksi (MPa)	f'_c, ksi (MPa)	ε ratio	Ψ ratio	δ ratio
1963 to 1999	$\rho = 0.75\,\rho_b$	Grade 60 (400 MPa)	8.45 (5450)	34 (234)	5 (34)	2.87	3.03	1.95
2002 and 2005	$\varepsilon_t = 0.005$	Grade 60 (400 MPa)	7.14 (4610)	39 (269)	5 (34)	3.71	3.44	1.81
2002 and 2005	$\varepsilon_t = 0.005$	Grade 70 (520 MPa)	5.71 (3680)	48 (331)	5 (34)	2.98	2.92	1.74
Proposed	$\varepsilon_t = 0.0066$	High-strength	2.43 (1570)	67 (462)	4 (28)	2.85	2.96	2.47
Proposed	$\varepsilon_t = 0.0066$	High-strength	2.86 (1850)	67 (462)	5 (34)	2.92	3.01	2.51
Proposed	$\varepsilon_t = 0.0066$	High-strength	3.21 (2070)	67 (462)	6 (41)	3.10	3.09	2.57
Proposed	$\varepsilon_t = 0.0066$	High-strength	3.71 (2390)	67 (462)	8 (55)	3.44	3.34	2.75
Proposed	$\varepsilon_t = 0.0066$	High-strength	4.64 (2920)	67 (462)	10 (69)	3.33	3.19	2.66

ε ratio = ratio of net tensile strain of steel at nominal strength to that at service load
Ψ ratio = ratio of beam curvature at nominal strength to that at service load
δ ratio = ratio of beam deflection at nominal strength to that at service load

Table 1.3: Specimen test matrix and results from Sumpter (2007).

Set	Beam ID	Spacing, in. (mm)	*a/d*	f'_c, psi (MPa)	V_{exp}, kips (kN)	$V_{exp}/(\sqrt{f'_c})bd$	Ratio of increment
1	C-C-6	6 (152)	2.62	3904 (26.9)	81.4 (364)	8.40	1.00
	C-M-6			4284 (29.5)	86.1 (383)	8.43	1.00
	M-M-6			4660 (32.1)	95.9 (426)	9.00	1.07
2	C-C-4	4 (102)	3.08	4390 (30.3)	83.1 (370)	8.04	1.00
	C-M-4			4547 (31.4)	91.3 (406)	8.68	1.08
	M-M-4			4704 (32.4)	101 (448)	9.40	1.17
3	C-C-3	3 (76.2)	3.08	4730 (32.6)	96.1 (427)	8.95	1.00
	C-M-3			4730 (32.6)	99.4 (442)	9.27	1.04
	M-M-3			4730 (32.6)	107 (476)	9.98	1.12

Table 1.4: AASHTO and ACI parameters for shear friction equations.

Surface condition	AASHTO				ACI		
					Given	Implied	
Parameter	***c* (ksi)**	***μ***	***K*$_1$**	***K*$_2$ (ksi)**	***μ***	***K*$_1$**	***K*$_2$ (ksi)**
Monolithically cast	0.40	1.4	0.25	1.5	1.4	0.20	0.80
Slabs on ¼" amplitude roughened surface	0.28	1.0	0.30	1.8	1.0	0.20	0.80
Other on ¼" amplitude roughened surface	0.24	1.0	0.25	1.5	1.0	0.20	0.80
Cast against surface with no roughening	0.075	0.6	0.20	0.8	0.6	0.20	0.80

Table 1.5: Test results from Kahn and Mitchell (2002) for cold-joint pushoff specimens.

Specimen identification no.	f'_c, psi (MPa)	$\rho_v f_y$, psi (MPa)	$\rho_v f_y$,* psi (MPa)	V_u, kips (kN)	v_u, psi (MPa)	$v_u/\sqrt{(f'_c)}$
SF-7-1-CJ	9347 (64.4)	304 (2.1)	220 (1.5)	54.0 (240.2)	900 (6.2)	9.3
SF-7-2-CJ	9347 (64.4)	609 (4.2)	440 (3.0)	82.1 (365.2)	1368 (9.4)	14.2
SF-7-3-CJ	10259 (70.7)	913 (6.3)	660 (4.6)	110.3 (490.6)	1838 (12.7)	18.1
SF-7-4-CJ	10259 (70.7)	1217 (8.4)	880 (6.1)	132.7 (590.2)	2211 (15.2)	21.8
SF-10-1-CJ	11117 (76.6)	304 (2.1)	220 (1.5)	31.7 (141.1)	529 (3.6)	5.0
SF-10-2-CJ	9515 (65.6)	609 (4.2)	440 (3.0)	49.3 (219.3)	822 (5.7)	8.4
SF-10-3-CJ	9485 (65.4)	913 (6.3)	660 (4.6)	113.9 (506.7)	1899 (13.1)	19.5
SF-10-4-CJ	9485 (65.4)	1217 (8.4)	880 (6.1)	126.0 (560.7)	2101 (14.5)	21.6
SF-14-1-CJ	12764 (88.0)	304 (2.1)	220 (1.5)	90.9 (404.4)	1515 (10.4)	13.4
SF-14-2-CJ	12764 (88.0)	609 (4.2)	440 (3.0)	99.2 (441.2)	1653 (11.4)	14.6
SF-14-3-CJ	12506 (86.2)	913 (6.3)	660 (4.6)	134.7 (599.2)	2245 (15.5)	20.1
SF-14-4-CJ	12506 (86.2)	1217 (8.4)	880 (6.1)	153.1 (681.1)	2552 (17.6)	22.8

*f_y = 60 ksi (414 MPa)

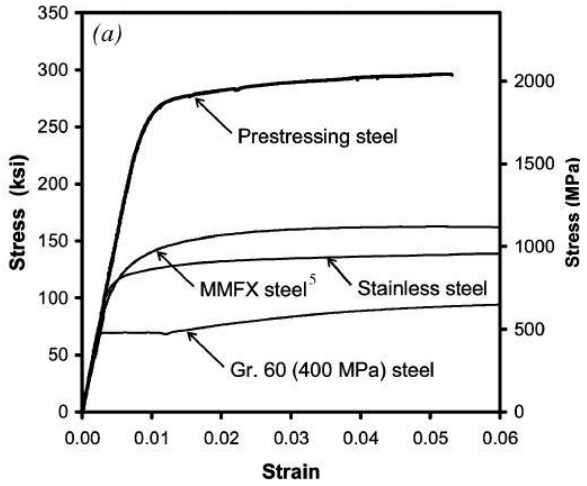

(a) Material characteristics of high-strength reinforcing steel.

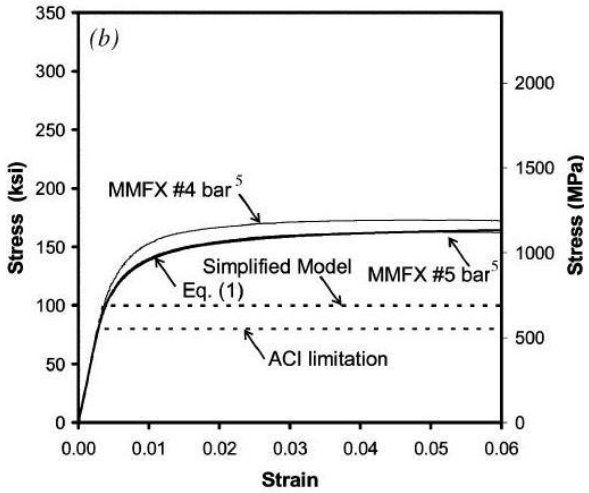

(b) MMFX stress-strain relationship models.

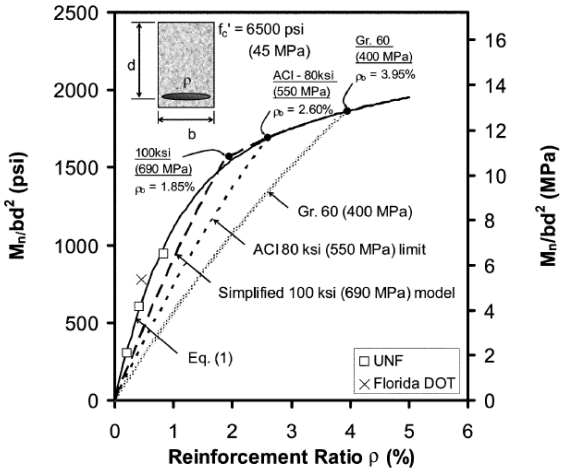

(c) Nominal moment capacity.

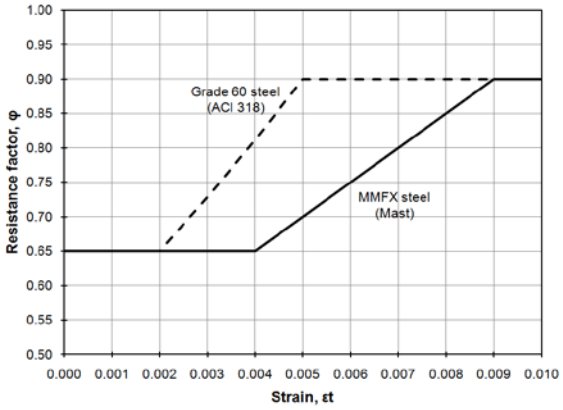

(d) Proposed variation of flexural resistance factor, φ, for the simplified design procedure.

Figure 1.1: Results from Mast et al. (2008).

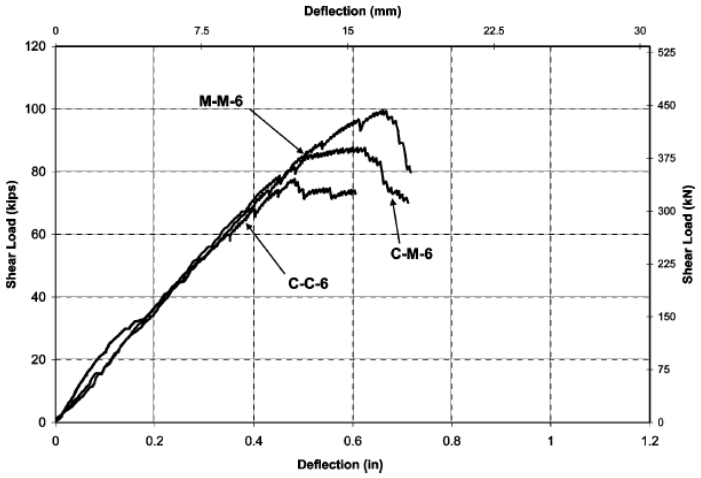

(a) Shear load-deflection relationship, Set 1

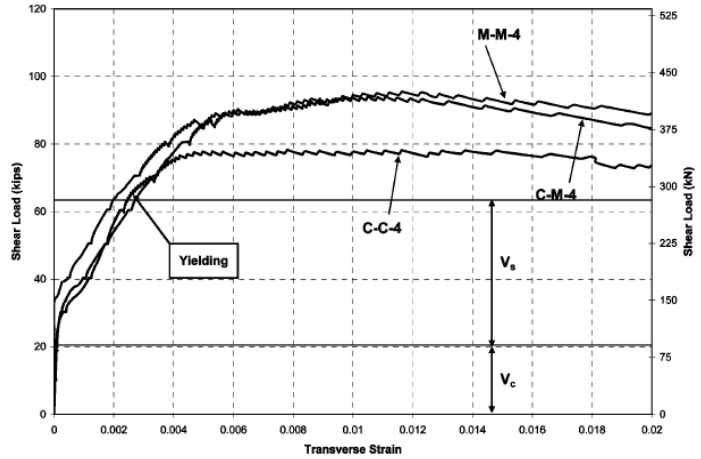

(b) Typical shear load-transverse strain relationship, Set 2

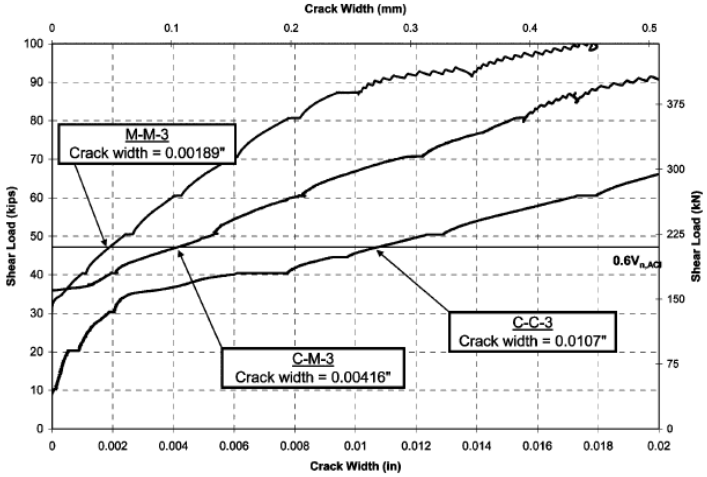

(c) Shear load-crack width relationship, Set 3

Figure 1.2: Results from Sumpter (2007).

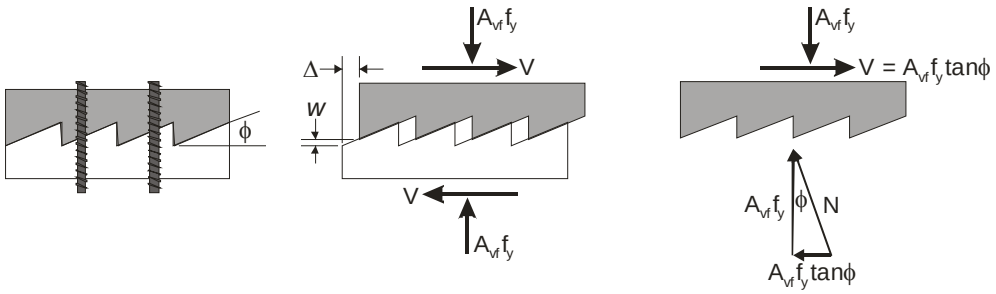

(a) Shear friction analogy as proposed by Birkeland and Birkeland (1966) (redrawn)

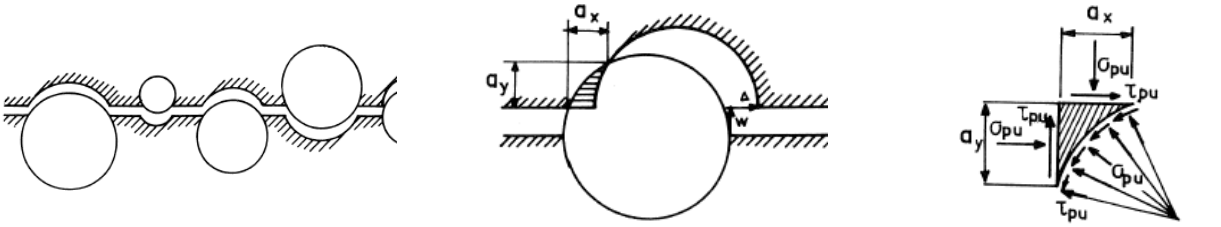

Idealized interface crack

Contact area between matrix and aggregate

Stress conditions in contact area

(b) Interfacial behavior described by Walraven and Reinhardt (1981)

Local restraint provided by reinforcing steel bond characteristics

Additional expected cracking

(c) Local behavior described by Walraven and Reinhardt (1981)

Figure 1.3: Representations of shear friction.

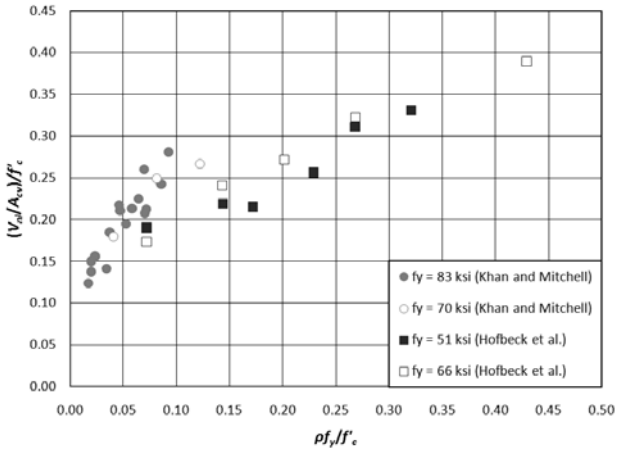

Figure 1.4: Normalized shear friction versus normalized interface reinforcing ratio.

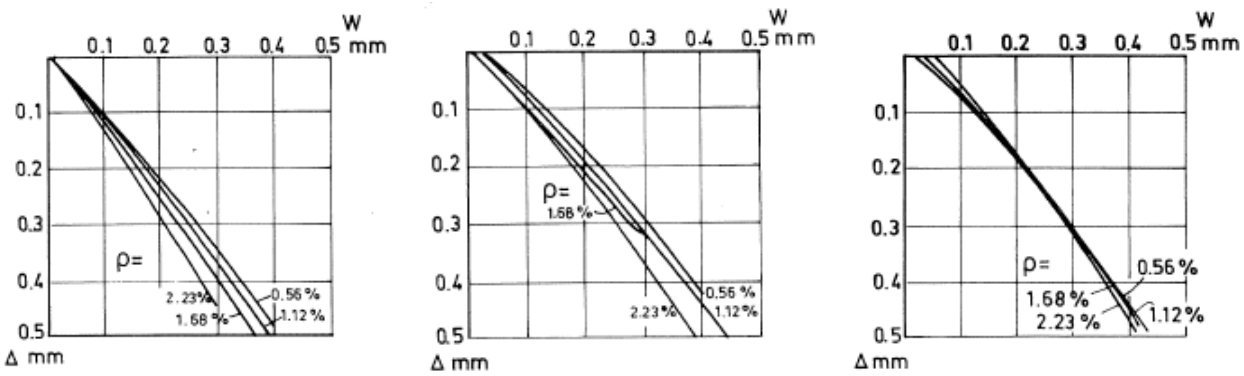

f'_c = 2.9 ksi f'_c = 4.5 ksi f'_c = 8.1 ksi

0.1 mm = 0.0039 in., 0.5 mm = 0.020 in

Figure 1.5: *Δ-w* relationships for varying interface reinforcing ratios.
(Walraven and Reinhardt, 1981)

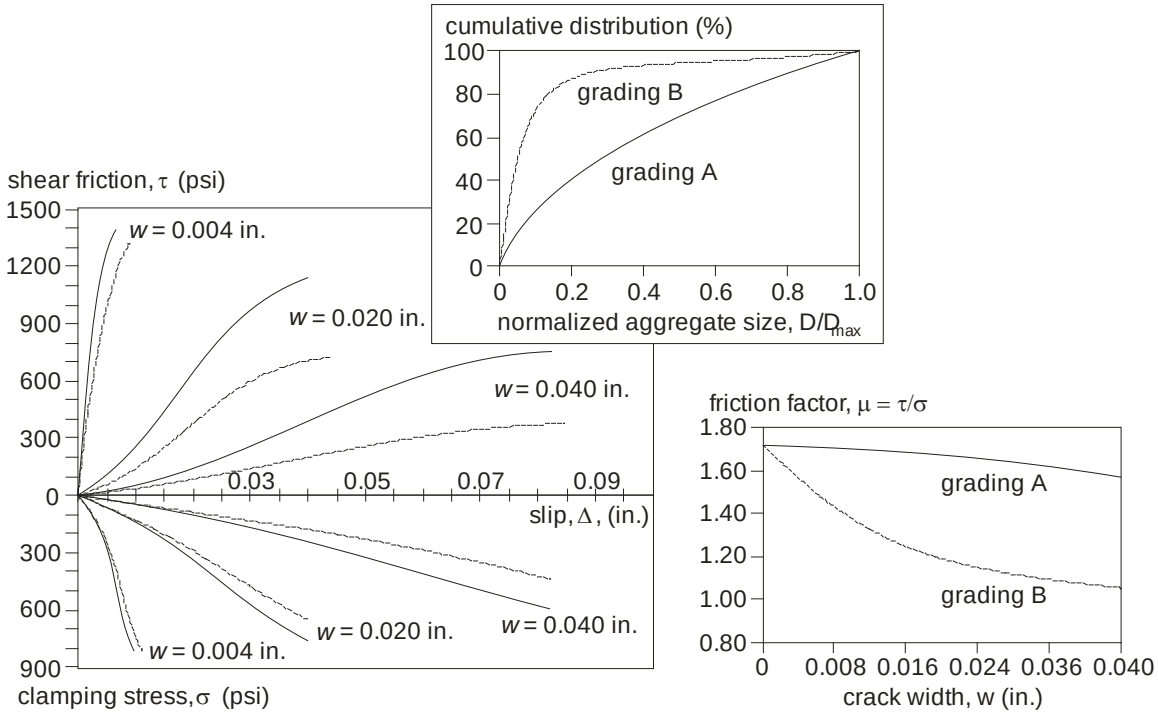

(a) shear and clamping stresses **(b)** friction coefficient

Figure 1.6: Role of crack width on interfacial stress development.
(Based on results from Walraven and Reinhardt 1981)

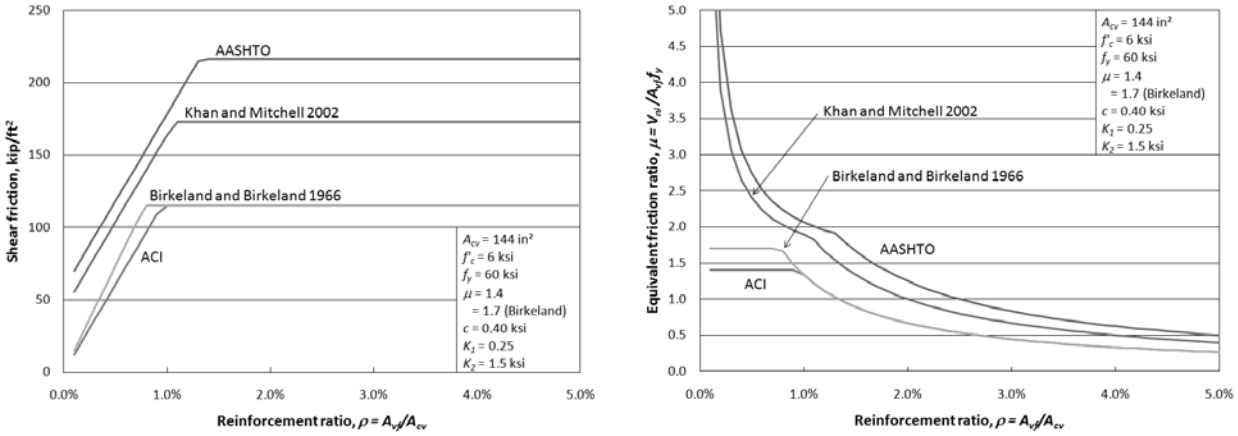

(a) Available shear friction per square foot **(b)** Equivalent friction factor

Figure 1.7: Shear friction values and friction factors determined from AASHTO and ACI.

2.0 EXPERIMENTAL PROGRAM

This experimental program is associated with Task 8.4b of the National Cooperative Highway Research Program (NCHRP) Project 12-77, *Structural Concrete Design with High-Strength Steel Reinforcement*. Its objective is to evaluate the effects of the use of high-strength steel reinforcement in shear friction applications. Typical push-off specimens, as shown in Figure 2.1, were used for the shear friction experiments performed as part of this program. This specimen geometry is commonly used (Walraven and Reinhardt 1981, Hofbeck et al. 1969, Kahn and Mitchell 2002) for such tests. The applied load is concentric with the test interface which is effectively subject to only shear stresses. The experiments consisted of applying a monotonically increasing load to the top and bottom surfaces of the specimens until the ultimate shear capacity of the test interface was reached. The shear is resisted by the concrete along the test interface and the steel ties crossing the interface. For these tests, the interface was placed as a 'cold joint' with the concrete on one side (designated as 1 in Figure 2.1) placed and allowed to cure prior to the placement of the other side of the interface (designated as 2 in Figure 2.1). The interface was horizontal during concrete placement, thus the interface may be thought of as representing the interface between a precast concrete girder and cast-in-place concrete deck. The interface steel reinforcement therefore represents the stirrup extensions or the interface shear reinforcement along such cold joint. The area of the concrete interface is represented by the term A_{cv} in Equations 1.3 and 1.4. The tie steel is anchored in the concrete to both sides of the interface and

serves to reinforce the interface. This interface steel is represented by the term A_{vf} in Equations 1.3 and 1.4. The parameters measured during the experiments were magnitude of the shear load, displacement parallel to the shear interface, crack width perpendicular to the shear interface, and strain in the steel reinforcement across the test interface. All these parameters were recorded throughout the entire test at a rate of 1 Hz.

2.1 SPECIMENS

The specimen designations, nominal material properties and measured material properties of the eight push-off specimens tested are shown in Table 2.1. Four types of duplicated specimens were tested, for a total of eight push-off tests performed. In the specimens labels, the letter “P” indicates the type of specimen (push-off), the numbers “615” and “1035” indicate the type of steel reinforcement (ASTM A615 and A1035 respectively), the numbers “3” and “4” indicate the size of the interface steel reinforcement (#3 (9.5 mm) and #4 (12.7 mm) respectively) and the letters “A” and “B” are used identify the duplicated specimens.

Construction of the specimens consisted of building the wooden forms and cutting the steel reinforcement, preparing and installing the strain gages, assembling the steel reinforcement cages and installing them inside the forms, placing and curing the first concrete cast, preparing the cold joint surface, and placing and curing the second concrete cast. Specimen dimensions and reinforcing details are shown in Figure 2.1.

Each specimen was built by first placing concrete in only a portion of the forms (designated as 1 in Figure 2.1) and 14 days later placing the two remaining portions (designated as 2 in Figure 2.1). The specimens were cast on their sides such that the resulting interface cold

joint was horizontal during casting. Between castings, the interface was cleaned of laitance and roughened to create a surface condition with ***at least*** ¼-inch amplitude in accordance with AASHTO 5.8.4.3 bullet one. Figure 2.2 shows an image of the resulting interface prior to placing cast 2. The resulting shear interface condition and concrete strength was based on the application of a connection between a composite slab and an AASHTO girder; the surface roughness is typical for this application and the 5 ksi concrete strength is appropriate for the slab. The presence of the additional cold joint in the loading block that is not part of the testing interface was required for constructability. This heavily cold joint was observed to have a negligible effect on the experiments based on its location and the path of the load during the experiments.

2.2 MATERIAL PROPERTIES

All measured concrete and steel reinforcing bar properties reported were obtained at the University of Pittsburgh as part of this test program except for the A1035 interface reinforcing bars used in specimens P-1035-3A and P-1035-4A which were tested at the University of Cincinnati.

A total of 21 test cylinders made with the two concrete mixes used in the push-off specimens were prepared and cured in accordance with ASTM A192/C192M-06. The cylinders were tested in accordance with ASTM C39/C39M-05 in order to determine the compressive strength of both concrete mixes. The design compressive strength, f'_c, for the concrete on both sides of the shear interface was 5 ksi (34.5 MPa). Measured concrete strengths at both 28 days and the age of testing are given in Table 2.1. The design of the concrete mixes is shown in Table 2.2 and the coarse aggregate grading curves are shown in Figure 2.3.

Two types of interface steel reinforcement were tested: ASTM A615 and A1035 with nominal yield strengths of 60 and 100 ksi (414 and 690 MPa), respectively. Two diameters of each steel type were tested: #3 (9.5 mm) and #4 (12.7 mm). All specimens had three double-legged ties crossing the interface; thus the interface reinforcing ratios were 0.0041 and 0.0075 for the specimens having #3 (9.5 mm) and #4 (12.7 mm) ties, respectively. Measured yield strength values of the interface steel reinforcement were verified to comply with the requirements of ASTM A615/A615M-06 and A1035/A1035M-07and are given in Table 2.1.

2.3 INSTRUMENTATION

The instrumentation used in the experiments consisted of three strain gauges, one located on each of the interface ties approximately 3 in. (75 mm) from the interface, and eight linear variable displacement transducers (LVDTs) as shown in Figure 2.4. A data acquisition system collected all strain and displacement data and the applied load from the testing machine.

2.4 TESTING

Testing consisted in using a compression machine to apply a monotonically increasing load to the top and bottom surfaces of the push-off specimens until the ultimate shear capacity of the test interface was reached. The load was applied through a 10 in. (250 mm) diameter plate at both the top and the bottom ends of the specimens; a ball-joint was used at the top to address small alignment discrepancies (none were observed in any test). A view of the test set-up is

shown in Figure 2.5. The load was applied at a rate of approximately 5000 lbs/min (22.2 kN/min). Once the ultimate shear capacity was reached, loading was continued in displacement control until the instrumentation failed due to spalling or excessive deformation of the specimens.

Table 2.1: Nominal and measured material properties of the push-off specimens.

Property		Specimen							
		P-615-3A	**P-615-3B**	**P-615-4A**	**P-615-4B**	**P-1035-3A**	**P-1035-3B**	**P-1035-4A**	**P-1035-4B**
Interface steel		6 #3 A615	6 #3 A615	6 #4 A615	6 #4 A615	6 #3 A1035	6 #3 A1035	6 #4 A1035	6 #4 A1035
$\rho_{min} = 0.05/f_y$		0.0008	0.0008	0.0008	0.0008	0.0005	0.0005	0.0005	0.0005
Nominal	f'_c	5000 psi (34.5 MPa) @ 28 days							
	A_{cv}	16 x 10 = 160 in^2 (103226 mm^2)							
	A_{vf}, in^2 (mm^2)	0.66 (426)	0.66 (426)	1.20 (774)	1.20 (774)	0.66 (426)	0.66 (426)	1.20 (774)	1.20 (774)
	$\rho = A_{vf}/A_{cv}$	0.0041	0.0041	0.0075	0.0075	0.0041	0.0041	0.0075	0.0075
	f_y	60 ksi (414 MPa)				100 ksi (689 MPa)			
Measured	f'_c	Cast #1: 6020 psi (41.5 MPa) @ 28 days; 7120 psi (49.1 MPa) @ 104 days (age at testing) Cast #2: 4220 psi (29.1 MPa) @ 28 days; 5800 psi (40.0 MPa) @ 90 days (age at testing)							
	A_{cv}, in^2 (mm^2)	160.4 (103484)	163.2 (105290)	165.0 (106451)	162.5 (104839)	157.5 (101613)	160.7 (103677)	162.5 (104839)	160.7 (103677)
	$\rho = A_{vf}/A_{cv}$	0.0041	0.0040	0.0073	0.0074	0.0042	0.0041	0.0074	0.0075
	f_y, ksi (MPa) (2% offset)	67.3 (464)	67.3 (464)	61.5 (424)	61.5 (424)	130.0[1] (896)	126.0 (869)	140.0[1] (965)	131.3 (905)
	f_u, ksi (MPa)	103.0 (710)	103.0 (710)	102.3 (705)	102.3 (705)	156.0[1] (1076)	157.6 (1087)	174.0[1] (1200)	172.3 (1188)
	ε_u	0.153	0.153	0.206	0.206	not recorded	0.111	not recorded	0.071

[1]bars tested at the University of Cincinnati

Table 2.2: Design of concrete mixes.

Material	Type	Quantity	Source	Specification
Cement	I	400 lb/yd^3	Essroc Cement	ASTM C 150
Fine Aggregate	Type A Sand	1346 lb/yd^3	Tri State River Products	ASTM C 33
Coarse Aggregate 1	#57 Gravel	1450 lb/yd^3	Tri State River Products	ASTM C 33
Coarse Aggregate 2	#8 Gravel	300 lb/yd^3	Tri State River Products	ASTM C 33
Pozzolan	C	175 lb/yd^3	Essroc Cement	ASTM C 618
Water	-	254 lb/yd^3	-	-
AE Agent	-	0 oz/yd^3	-	ASTM C 260
WR Agent	800 N	4 oz/cwt	Axim Concrete Tech.	ASTM C 494

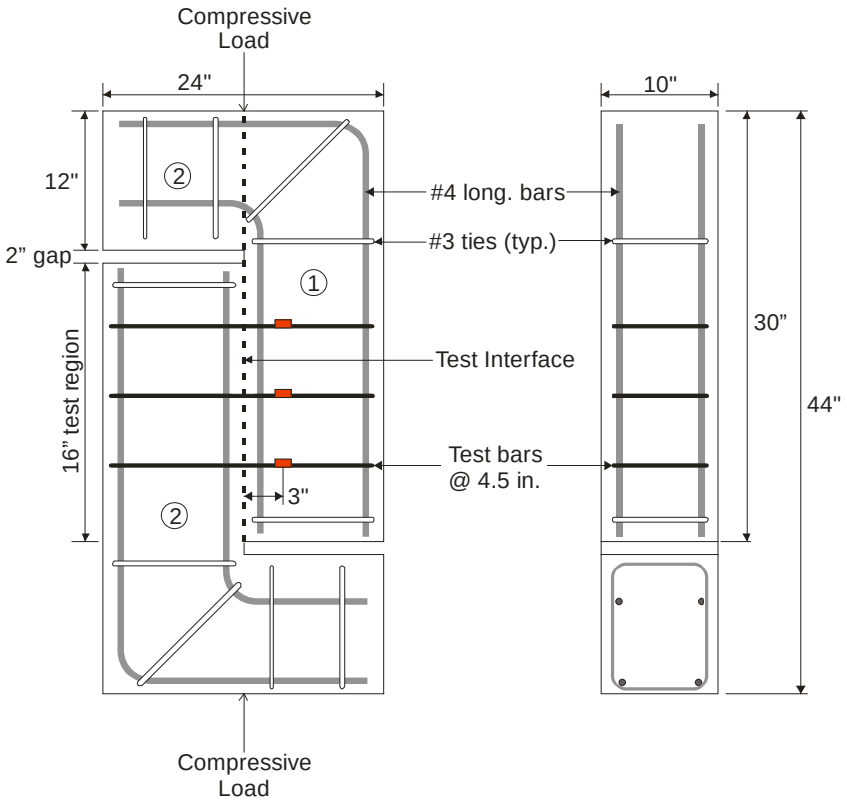

Figure 2.1: Push-off specimen dimensions and reinforcing details.

(a) Typical interface surface; Concrete Repair Institute standard surface profile chip #9 (CSP9) shown at right of image.

(b) Typical interface surface.

Figure 2.2: Interface condition prior to placing cast 2.

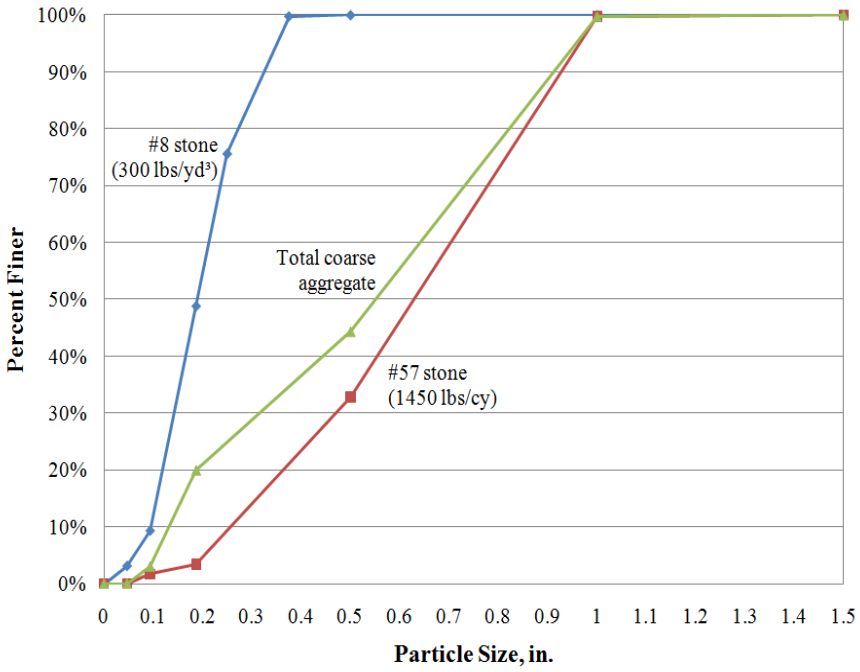

Figure 2.3: Coarse aggregate grading curves for concrete mixes.

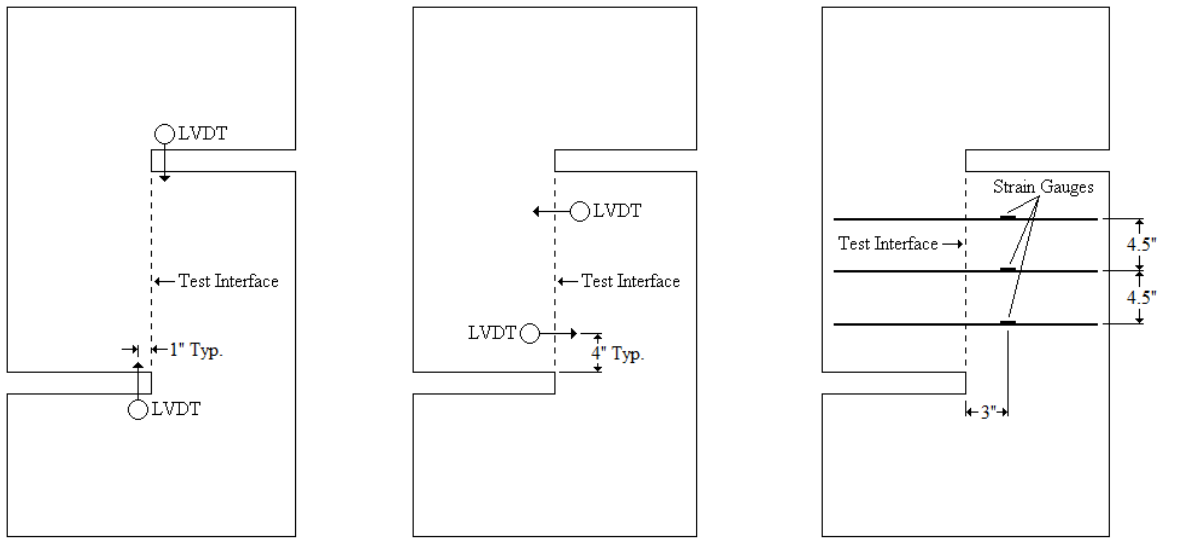

(a) Shear displacement instrumentation (both sides)

(b) Crack width instrumentation (both sides)

(c) Interface steel reinforcement strain instrumentation

Figure 2.4: Detail of instrumentation.

(a) Specimen prior to testing

(b) Specimen following testing. Displacement along shear interface can be seen as displaced horizontal lines representing interface reinforcement locations.

Figure 2.5: Test set-up.
(Specimen P-615-3B shown)

3.0 EXPERIMENTAL RESULTS

The following experimental results are based on the parameters measured during the push-off tests. These were the magnitude of the shear load, the shear displacement parallel to the test interface, the crack width perpendicular to the test interface, and the strain in the steel reinforcement across the test interface. The results for shear load, V, shear displacement, Δ, crack width, w, and interface steel reinforcement strain, ε_s, for each individual specimen, as well as the average between pairs of duplicated specimens, at the cracking and ultimate shear loads are shown in Tables 3.1 and 3.2, respectively. In addition, the load-displacement (V-Δ), load-crack width (V-w) and load-interface steel reinforcement strain (V-ε_s) plots of all specimens are shown in Figures 3.2 through 3.4, respectively, with a comparison of the plots from all the specimens shown in Figure 3.5. As can be seen from these figures, duplicate instruments generally tracked each other very well; thus average values of shear displacement and crack width are generally reported (occasionally bad gages are removed from the data set; these are noted in the figures). Figure 3.6 shows some examples of observed test behavior. These images are taken well after the ultimate load is achieved. As is described below, the ultimate load corresponds to very small displacements/distortions which cannot be seen in photographs.

3.1 SHEAR LOAD

Two important shear load values were monitored during the push-off experiments; the load to cause the initial shear crack, referred to as the 'cracking shear load', V_{crack}, and the highest shear capacity obtained, referred to as the 'ultimate shear load', V_u. The cracking shear load is the force necessary to break the bond between the two concrete surfaces that form the shear interface. After this load is attained, shear friction dominates the behavior of the loaded specimen until the ultimate shear load is achieved. As explained in Section 1.2.1, the shear friction mechanism arises from the roughness of the concrete interface and a clamping force created by the interface reinforcement, which restrains crack opening. After the ultimate shear load is achieved the specimen continues to deflect with no further increase in capacity. The crack width increases, reducing the friction component although theoretically increasing the clamping force. Additionally, the roughness of the shear interface is reduced due to shearing off of the local asperities.

The cracking shear load, V_{crack}, for each specimen was obtained from the load-crack width (*V*-*w*) plots, which showed a disturbance in all LVDT readings at approximately the load at which cracking of the shear interface was first observed. An example of the load-crack width plot used to approximate the cracking shear load of specimen P-615-3A is shown in Figure 3.1. The cracking shear load for each specimen is shown in Table 3.1, which shows that, on average, cracking of the shear interface in the specimens occurred at a load of 61 kips (272 kN), or at a concrete stress of 0.38 ksi (2.6 MPa). Traditionally, concrete shear strength is given as a function of $\sqrt{f'_c}$ The observed cracking shear is therefore $5\sqrt{f'_c}$ (psi) ($0.41\sqrt{f'_c}$ (MPa)), based on the lower concrete strength at the interface: f'_c = 5800 psi (40 MPa).

As can be seen from Table 3.1 and Figure 3.4, the stress in the reinforcing steel at the point of shear cracking is negligible and therefore not significantly contributing to the shear capacity up to the instant of cracking.

The ultimate shear load, V_u, for each specimen was established using both the maximum applied load recorded by the testing machine during the push-off experiments and the load-displacement (V-Δ) plots of the specimens, which are shown in Figure 3.2. As can be seen in Figure 3.2, the ultimate shear load can be easily identified in the specimens reinforced with ASTM A615 steel since they exhibit a very noticeable peak, followed by a rapid drop in their load capacity. However, the specimens reinforced with ASTM A1035 steel exhibit a much different behavior in their load-displacement history plots, which essentially 'plateau' after a certain load value. The load value at the beginning of this plateau was taken as the ultimate shear load, based on the previous explanation of the shear friction mechanism. The ultimate shear load for each specimen is shown in Table 3.2, which shows that the pairs of specimens with #4 (12.7 mm) steel reinforcement exhibited greater shear friction capacity than those with #3 (9.5 mm) reinforcement. From Table 3.2 it can also be seen that, considering reinforcement size, the pairs of specimens reinforced with ASTM A1035 steel have approximately the same capacity as those reinforced with ASTM A615 steel; this will be discussed further in Chapter 4.

3.2 SHEAR DISPLACEMENT

From Tables 3.1 and 3.2 it can be seen that there is significant variability between the individual shear displacement values of all the specimens; between 0.006 and 0.011 in. (0.163 and 0.270 mm) at the cracking shear load and between 0.025 and 0.041 in. (0.642 and 1.039 mm)

at the ultimate shear load. This behavior can also be seen in Figure 3.5.a, which shows the plots for all the specimens reaching their ultimate shear load at a relatively broad range of shear displacements. This variability appears to be related to the size of the interface steel reinforcement, since the pairs of specimens with #3 (9.5 mm) steel reinforcement have similar displacement values, but different from the displacement values of the pairs of specimens with #4 (12.7 mm) steel reinforcement.

In terms of the average shear displacement between the pairs of duplicated specimens it can be seen that the pairs with #3 (9.5 mm) interface steel reinforcement exhibited greater shear displacement than those with #4 (12.7 mm) steel reinforcement at the cracking shear load, which was similar for all specimens. However, at the ultimate shear load, which was higher for the pairs of specimens with #4 (12.7 mm) steel reinforcement, these exhibited greater shear displacement than those with #3 (9.5 mm) steel reinforcement. This result should be expected due to the load-displacement relationship (i.e. the higher the load, the greater the displacement).

3.3 CRACK WIDTH

From Tables 3.1 and 3.2 it can be seen that the crack width values at the cracking and ultimate shear loads show less variability than the shear displacement values; negligible crack width at the cracking shear load and between 0.007 and 0.010 in. (0.166 and 0.246 mm) at the ultimate shear load. This behavior can also be seen in Figure 3.5.b, which shows the plots for all the specimens reaching their ultimate shear load at a relatively narrow range of crack widths values. Again, the variability appears to be related to the size of the interface steel reinforcement since the pairs of specimens with #3 (9.5 mm) steel reinforcement have similar crack width

values, but different from the values of the pairs of specimens with #4 (12.7 mm) steel reinforcement.

As seen with the average shear displacement, the pairs of duplicated specimens with #3 (9.5 mm) steel reinforcement exhibited greater crack widths at the cracking shear load than those with #4 (12.7 mm) steel reinforcement. In addition, the pairs of specimens with #4 (12.7 mm) steel reinforcement exhibited greater crack widths at the ultimate shear load than those with #3 (9.5 mm) steel reinforcement, which again, is likely due to the load-displacement proportionality.

3.4 INTERFACE STEEL REINFORCEMENT STRAIN

From Tables 3.1 and 3.2 it can be seen that, as with the shear displacement, the interface steel reinforcement strain values at the cracking and ultimate shear loads vary significantly between specimens; between 23 and 61 με at the cracking shear load and between 222 and 579 με at the ultimate shear load. This behavior can also be seen in Figure 3.5.c, which shows the plots for all the specimens reaching their ultimate shear load at a relatively broad range of interface steel reinforcement strain values. As with the shear displacement, the variability appears to be related to the size of the interface steel reinforcement, since the pairs of specimens with #3 (9.5 mm) steel reinforcement have similar interface steel reinforcement strain values, but different from the values of the pairs of specimens with #4 (12.7 mm) steel reinforcement. However, the type of steel reinforcement appears to contribute to the variability of the values as well, since the specimens with ASTM A615 steel reinforcement have slightly lower interface steel reinforcement strain values than the specimens with ASTM A1035 steel reinforcement of

the same size. This behavior is possibly due to the enhanced bond characteristics of ASTM A1035 steel described in Section 1.1.3.

In order to be reliable and unaffected by the crack opening, all strain data is obtained at a location about 3 inches (75 mm) from the interface. Thus the actual bar strain at the interface is expected to be greater as some of the bar stress is transmitted back into the concrete over this short development length. As the concrete is damaged during testing (see Figures 1.3.c and 3.6.b), the difference in strain between the interface and measurement location is expected to be become less significant.

Table 3.1: Summary of average values recorded at the cracking shear load.

Specimen	V_{crack}, kips (kN)	Avg.	$\tau = V/A_{cv}$, ksi (MPa)	Avg.	Δ, in (mm)	Avg.	w, in (mm)	Avg.	ε_s, με	Avg.	$\sigma_s = E_s\varepsilon_s$, ksi (MPa)	Avg.
P-615-3A	66.2 (294.5)	66.5 (295.8)	0.41 (2.8)	0.41 (2.8)	0.008 (0.21)	0.009 (0.24)	0.001 (0.01)	0.000 (0.012)	23	27	0.68 (4.7)	0.77 (5.3)
P-615-3B	66.8 (297.1)		0.41 (2.8)		0.010 (0.27)		0.000 (0.01)		30		0.87 (6.0)	
P-615-4A	50.0 (222.4)	54.1 (240.6)	0.30 (2.1)	0.33 (2.3)	0.006 (0.16)	0.007 (0.18)	0.000 (0.01)	0.000 (0.010)	27	27	0.78 (5.4)	0.79 (5.5)
P-615-4B	58.2 (258.9)		0.36 (2.5)		0.007 (0.19)		0.000 (0.01)		28		0.81 (5.6)	
P-1035-3A	57.2 (254.6)	64.9 (288.6)	0.36 (2.5)	0.41 (2.8)	0.009 (0.24)	0.010 (0.25)	0.000 (0.01)	0.001 (0.014)	38	40	1.11 (7.7)	1.16 (8.0)
P-1035-3B	72.5 (322.6)		0.45 (3.1)		0.011 (0.27)		0.001 (0.02)		42		1.21 (8.3)	
P-1035-4A	58.4 (260.0)	59.2 (263.4)	0.36 (2.5)	0.37 (2.5)	0.007 (0.17)	0.008 (0.20)	0.000 (0.01)	0.000 (0.011)	24	43	0.70 (4.8)	1.24 (8.5)
P-1035-3B	60.0 (266.7)		0.37 (2.6)		0.009 (0.23)		0.001 (0.02)		61		1.78 (12.3)	
Avg.	**61.2 (272.1)**		**0.38 (2.61)**									

Table 3.2: Summary of average values recorded at the ultimate shear load.

Specimen	V_u, kips (kN)	Avg.	$\tau = V/A_{cv}$, ksi (MPa)	Avg.	Δ, in (mm)	Avg.	w, in (mm)	Avg.	ε_s, με	Avg.	$\sigma_s = E_s\varepsilon_s$, ksi (MPa)	Avg.
P-615-3A	112.5 (500.2)	104.5 (464.7)	0.70 (4.8)	0.65 (4.5)	0.025 (0.64)	0.026 (0.66)	0.008 (0.21)	0.008 (0.20)	238	322	6.92 (47.7)	9.33 (64.3)
P-615-3B	96.5 (429.2)		0.59 (4.1)		0.027 (0.68)		0.007 (0.19)		405		11.74 (80.9)	
P-615-4A	114.5 (509.1)	121.7 (541.5)	0.69 (4.8)	0.74 (5.1)	0.037 (0.94)	0.037 (0.95)	0.009 (0.22)	0.008 (0.21)	515	463	14.93 (102.9)	13.41 (92.5)
P-615-4B	129.0 (573.8)		0.79 (5.5)		0.038 (0.97)		0.008 (0.20)		410		11.90 (82.0)	
P-1035-3A	90.0 (400.3)	97.5 (433.7)	0.57 (3.9)	0.61 (4.2)	0.027 (0.68)	0.029 (0.73)	0.007 (0.17)	0.007 (0.19)	222	375	6.44 (44.4)	10.87 (74.9)
P-1035-3B	105.0 (467.0)		0.65 (4.5)		0.031 (0.78)		0.008 (0.21)		527		15.29 (105.4)	
P-1035-4A	135.7 (603.6)	124.6 (554.3)	0.84 (5.8)	0.77 (5.3)	0.032 (0.80)	0.036 (0.92)	0.008 (0.21)	0.009 (0.23)	529	554	15.35 (105.9)	16.07 (110.8)
P-1035-3B	113.5 (505.0)		0.71 (4.9)		0.041 (1.04)		0.010 (0.25)		579		16.79 (115.8)	

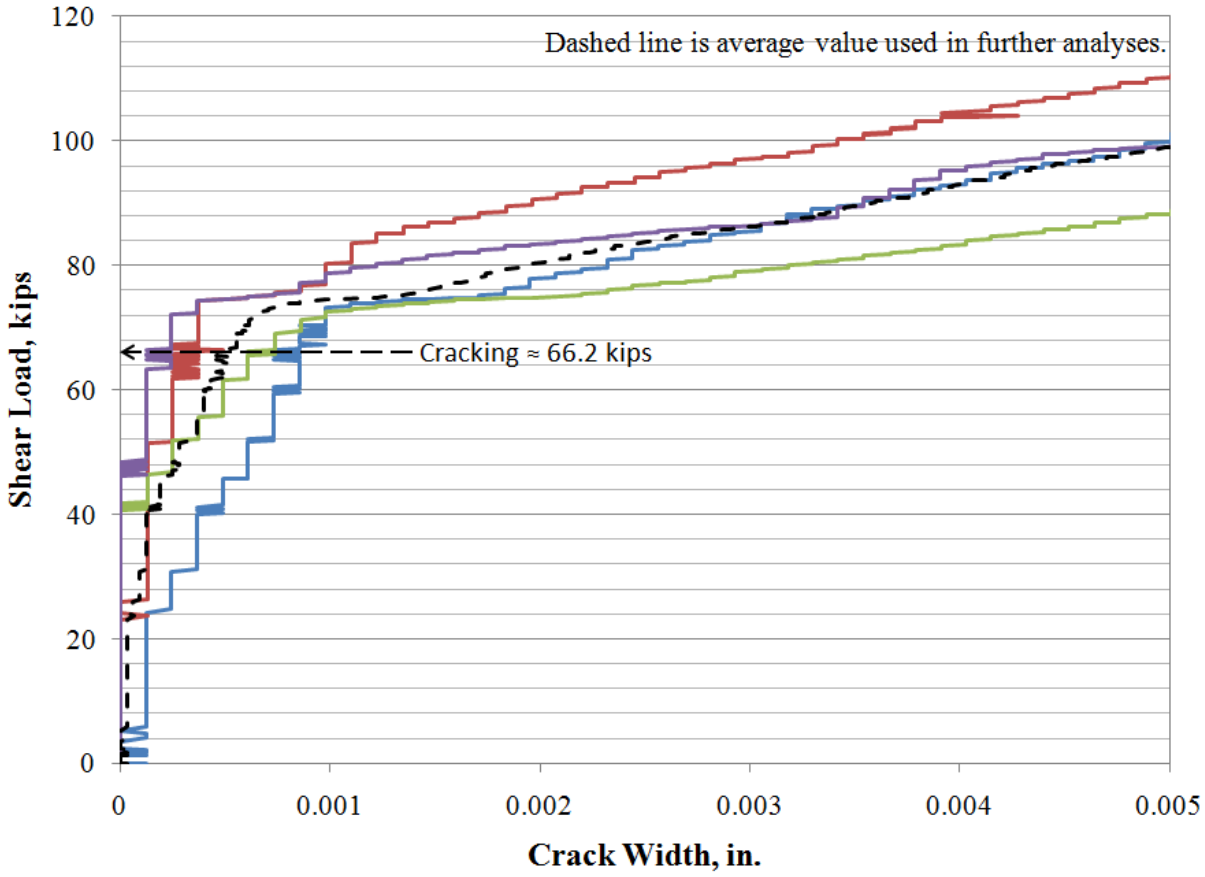

Figure 3.1: Approximation of cracking shear load.
(Results for specimen P-615-3A shown)

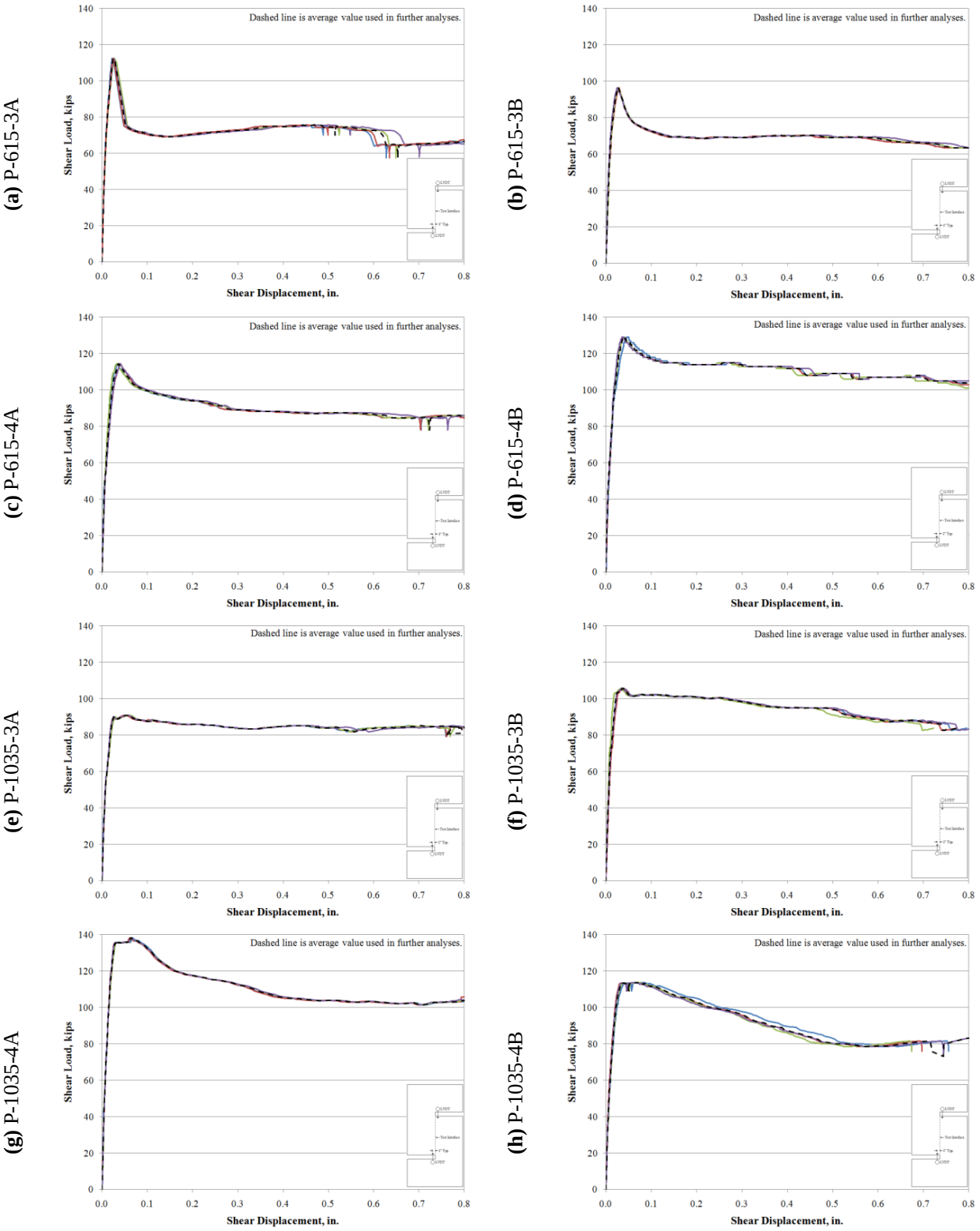

Figure 3.2: Experimental results for shear load versus shear displacement.

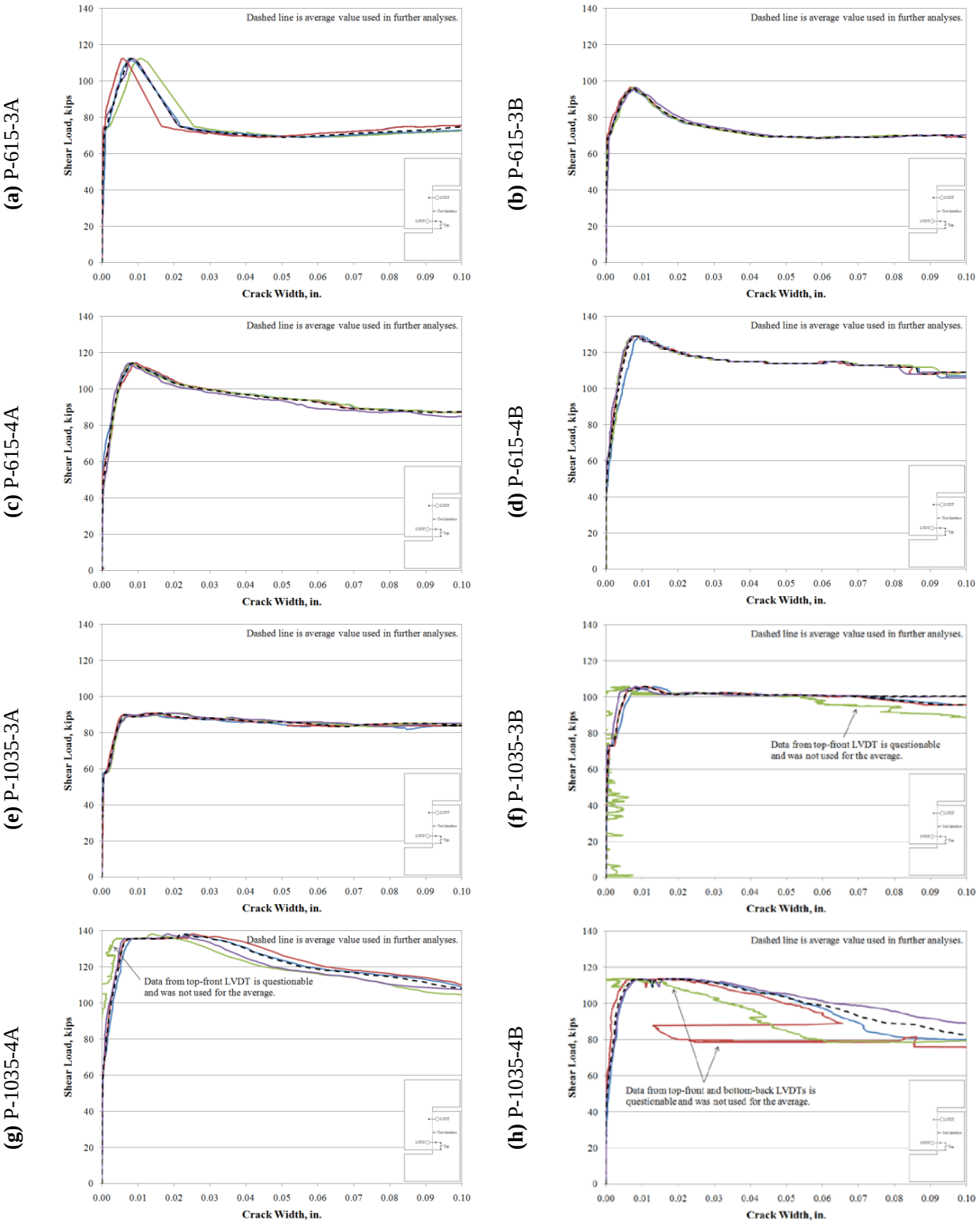

Figure 3.3: Experimental results for shear load versus crack width.

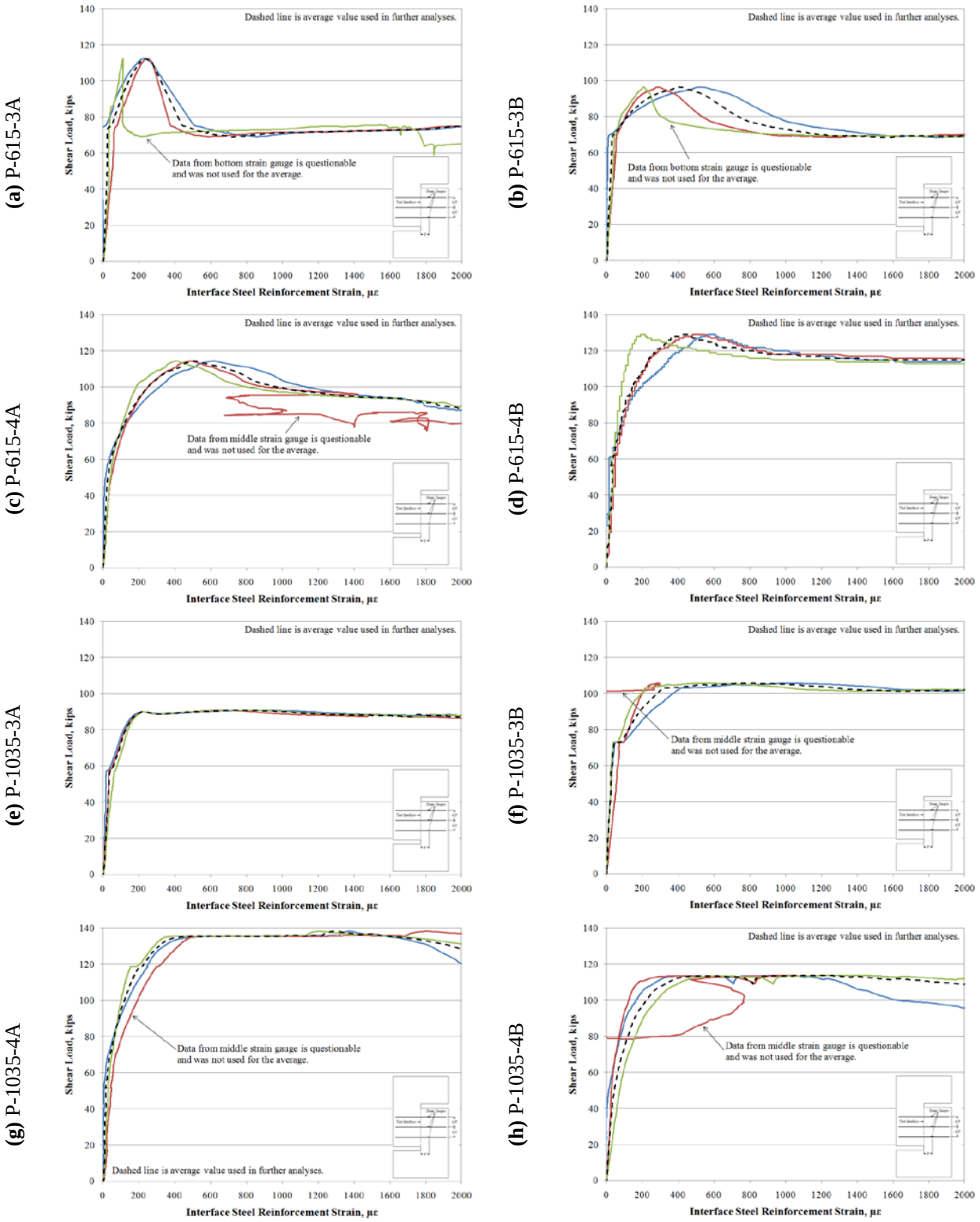

Figure 3.4: Experimental results for shear load versus interface steel reinforcement strain.

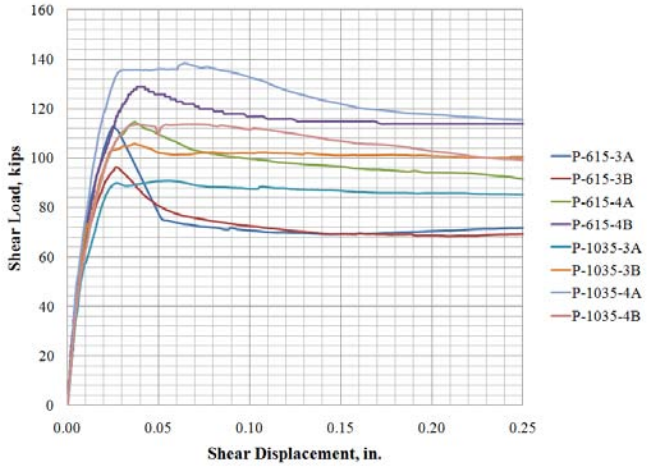

(a) Shear load versus average shear displacement

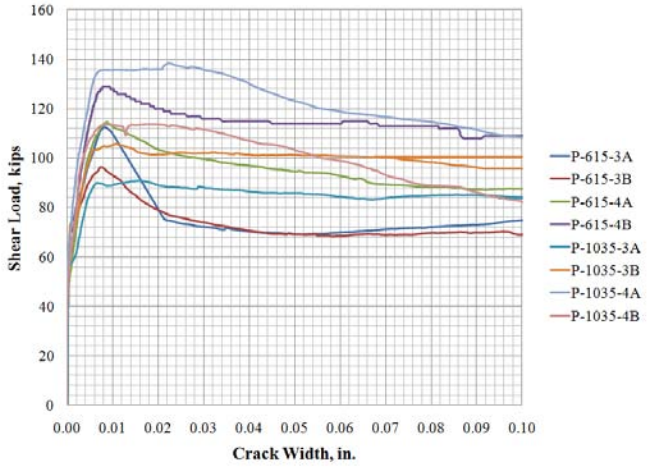

(b) Shear load versus average crack width

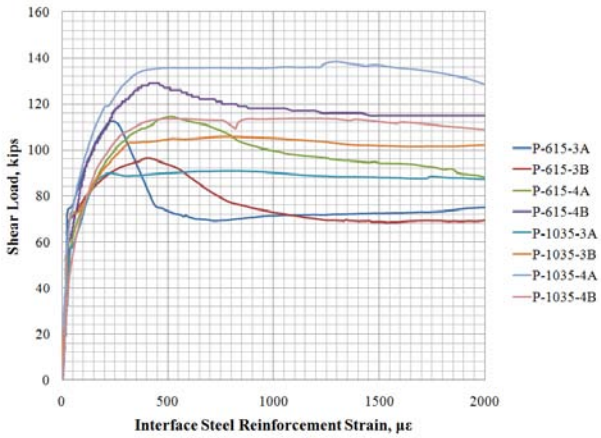

(c) Shear load versus average interface steel strain

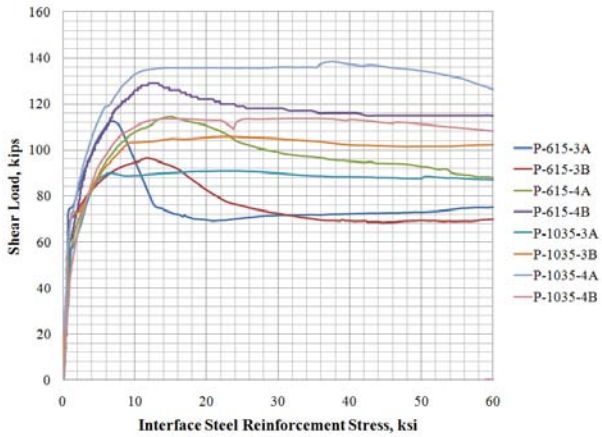

(d) Shear load versus average interface steel stress

Figure 3.5: Comparison of test results for each specimen.

(a) P-615-3B at a slip exceeding 1 in. (25 mm). Displacement along shear interface can be seen as displaced horizontal lines representing interface reinforcement locations.

(b) Distortion of the interface steel reinforcement of specimen P-1035-3A following large slip.

Figure 3.6: Images from testing.

4.0 DISCUSSION

The following discussion is based on the experimental findings as well as comparisons between the calculated and experimental capacities of the push-off specimens. Data from previous research work, which is discussed as part of the literature review, will be used to support the discussion.

4.1 CALCULATED VERSUS EXPERIMENTAL CAPACITIES

4.1.1 AASHTO and ACI

The AASHTO LRFD (2007) and ACI 318 (2008) equations for calculating the nominal shear friction capacity of a concrete interface, V_{ni}, are repeated below. It is noted that in both of these equations, the yield strength, f_y, of the interface shear reinforcement is limited to 60 ksi (414 MPa). Additionally, recall that AASHTO uses units of ksi for all stresses while ACI uses units of psi.

AASHTO 5.8.4:

$$V_{ni} = cA_{cv} + \mu(A_{vf}f_y + P_c) \quad \text{(Eq. 4.1)}$$

$$V_{ni} \leq K_1 f'_c A_{cv}$$

$$V_{ni} \leq K_2 A_{cv}$$

ACI 318 11.7.4:

$$V_{ni} = A_{vf} f_y \mu \quad \text{(Eq. 4.2)}$$

$$V_{ni} \leq 0.20 f'_c A_{cv}$$

$$V_{ni} \leq 800 A_{cv}$$

The shear friction capacity of the push-off specimens was calculated using Equations 4.1 and 4.2. A summary of experimental results is presented in Table 4.1. The calculated capacities as well as the ratios between the measured and the calculated capacities using both the measured yield strength value of the interface steel reinforcement (see Table 2.1) and the limitation of 60 ksi are shown in Tables 4.2 and 4.3. The capacities were calculated using the measured area of the concrete shear interface, A_{cv}, and measured concrete compressive strength shown in Table 2.1. In addition, based on AASHTO and ACI guidance, the following values were used to calculate the capacities:

μ = 1.0 (AASHTO friction factor or ACI coefficient of friction);

c = 0.24 ksi (cohesion factor);

K_1 = 0.25 (fraction of concrete strength available to resist interface shear); and

K_2 = 1.5 ksi (limiting interface shear resistance).

From Tables 4.2 and 4.3 it can be seen that the shear friction capacity, V_{ni}, calculated using Equations 4.1 and 4.2, respectively, is less than the measured capacity or ultimate shear load, V_u, for all specimens when the interface steel reinforcement yield strength, f_y, is limited to 60 ksi as required by AASHTO LRFD (2007) and ACI 318 (2008). Thus both equations appear to be conservative for the cases considered when the yield strength value is limited to 60 ksi. However, from the ratios of ultimate shear load to calculated capacity, V_u/V_{ni}, it can be seen that both equations become less conservative as the area of interface steel reinforcement, A_{vf},

increases. This is a result of the implication in the equations that the steel reinforcement is yielding at the ultimate shear load which, as shown in Table 3.2, is not correct. As a result, the increase in capacity due to the increase in interface steel reinforcement area is overestimated.

When the capacity of the specimens is calculated with Equations 4.1 and 4.2 using the interface steel reinforcement measured yield strength, ignoring the fact that both AASHTO LRFD (2007) and ACI 318 (2008) limit the interface steel reinforcement yield strength to a maximum of 60 ksi, the calculated capacity of some of the specimens with ASTM A1035 interface steel reinforcement is greater than the measured capacity. Again, this is because both equations imply that the steel reinforcement is yielding at the ultimate shear load, which is not correct. Furthermore, as shown in Table 3.2, the steel stress at the ultimate shear load is similar regardless of the steel grade. This result should be expected since the steel stress is a function of the steel modulus (constant regardless of grade) and the crack opening dimension which is primarily a function of the concrete aggregate size (see Figure 1.3). As a result, an increase in capacity due to the increase in interface steel reinforcement yield strength does not occur. Therefore, it can be seen that in order to obtain conservative results with Equations 4.1 and 4.2, the use of the 60 ksi limitation on the interface steel reinforcement is warranted. It will be shown, however, that even this limitation is arbitrary and is simply an empirical fit to the available data. The implication in Equations 4.1 and 4.2 that the steel yields at the ultimate shear capacity is simply not true but empirically limiting the yield strength value to 60 ksi results in a good and moderately conservative estimation of shear capacity as it has done in this study.

This final point is demonstrated in Figure 4.1, which shows the load-crack width (V-w) plots along with the steel and concrete components of the measured shear friction capacity for all the specimens. The steel component was calculated using the measured interface steel

reinforcement strain to calculate the actual steel stress and assumes a friction factor, μ, equal to 1.0. The concrete component was calculated by subtracting the steel component from the applied shear load; this is referred to as the 'apparent concrete component'. Figure 4.1 also shows the calculated capacity for all the specimens, obtained using Equation 4.1 taking f_y equal to the measured yield strength of the interface steel reinforcement instead of the 60 ksi limitation, as well as the nominal concrete and steel components, cA_{cv} and $\mu A_{vf} f_y$, of the calculated capacity. From the plots in Figure 4.1 it can be seen that:

- At its peak, the apparent concrete component greatly exceeds the nominal concrete component (cA_{cv} term in Equation 4.1) and contributes the majority of the shear friction capacity of the specimens.
- The steel component is significantly lower than the nominal steel component ($\mu A_{vf} f_y$ term in Equation 4.1), and reaches its peak value well after the shear friction capacity of the specimens is exceeded.
- By the time the steel component reaches its peak value, the apparent concrete component is significantly lower than its peak value **and** the nominal concrete component, cA_{cv}.
- The calculated shear friction capacity exceeds the measured capacity of all the specimens with ASTM A1035 interface steel reinforcement when the measured yield strength of the interface steel reinforcement is used instead of the 60 ksi limitation.

These findings demonstrate that Equations 4.1 and 4.2 do not represent the shear friction mechanism accurately since both imply that the maximum concrete and steel components of the shear friction occur simultaneously. In fact, as seen in Figure 4.1 the concrete component

contributes to the majority of the shear friction capacity before the ultimate shear load is reached and then decreases to a residual value while the steel component increases. However, the steel component never reaches its peak value, $\mu A_{vf} f_y$, before the ultimate shear load is reached. Therefore, both equations neglect the staged behavior of the shear friction mechanism and arbitrary and simply fit the data used to establish them empirically.

It is noted that this discussion has assumed a friction factor, μ, equal to 1. This is arbitrary, although the data will simply be shifted linearly if a different value is used. Assuming a friction factor value is necessary to resolve the concrete component from an otherwise indeterminate equation.

4.1.2 Birkeland and Birkeland (1966)

The equation proposed by Birkeland and Birkeland (1966) to calculate the nominal shear friction capacity of a concrete interface, V_{ni}, is:

$$V_{ni} = A_{vf} f_y \tan \varnothing \qquad \text{where:} \qquad \tan \varnothing = \begin{cases} 1.7 \text{ for monolitic concrete} \\ 1.4 \text{ for artificially roughened joints} \\ 1.0 \text{ for ordinary joints} \end{cases} \qquad \text{(Eq. 4.3)}$$

From Table 4.4 it can be seen that the shear friction capacity, V_{ni}, calculated using Equation 4.3 is less than the measured capacity or ultimate shear load, V_u, for all the specimens when the interface steel reinforcement yield strength, f_y, is limited to 60 ksi. This result is expected since Equation 4.3 only differs from the ACI equation (Equation 4.2) in the recommended values of the coefficient of friction and therefore appears to be conservative for the cases considered when the yield strength value is limited to 60 ksi. However, as with the ACI equation, from the ratios of ultimate shear load to calculated capacity, V_u/V_{ni}, in Table 4.4 it can be seen that Equation 4.3 becomes less conservative as the area of interface steel reinforcement, A_{vf}, increases. As

explained previously the reduction in conservativeness results from the implication that the steel reinforcement is yielding at the ultimate shear load which, as shown in Table 3.2, is not correct. As a result, the increase in capacity due to the increase in interface steel reinforcement area is overestimated. Furthermore, when the capacity of the specimens is calculated with Equation 4.3 using the interface steel reinforcement measured yield strength, the calculated capacity of some of the specimens with ASTM A1035 interface steel reinforcement is greater than the measured capacity. Again, this is because the equation implies that the steel reinforcement is yielding at the ultimate shear load, which is not correct.

4.1.3 Kahn and Mitchell (2002)

The equation proposed by Kahn and Mitchell (2002) to calculate the nominal shear friction capacity of a concrete interface, V_{ni}, is:

$$V_{ni} = 0.05A_{cv}f'_c + 1.4A_{vf}f_y \leq 0.2A_{cv}f'_c \quad \text{(Eq. 4.4)}$$

From Table 4.5 it can be seen that the shear friction capacity, V_{ni}, calculated using Equation 4.4 is greater than the measured capacity or ultimate shear load, V_u, for six of the eight specimens tested, even when the interface steel reinforcement yield strength, f_y, is limited to 60 ksi. These results show that Equation 4.4, which is a modification of the AASHTO equation (Equation 4.1) intended to be applicable to high strength concrete, provides nonconservative results for the cases considered, even if the yield strength value is limited to 60 ksi. This is likely because the coefficients in Equation 4.4 are empirical and were selected to fit the data used to establish the equation. In addition the equation also implies that the steel reinforcement is yielding at the ultimate shear load, which as mentioned previously is not correct.

4.2 OBSERVED SHEAR FRICTION BEHAVIOR

The experimental data for all the push-off specimens shows that the shear friction mechanism can be divided into three stages. These stages are depicted in Figure 4.2, which shows the load-displacement (V-Δ), load-crack width (V-w) and load-interface steel reinforcement strain (V-ε_s) plots for all the specimens, as well as a linearization of each of these plots for illustration purposes. The three stages of behavior are described as follows:

4.2.1 Stage 1: Pre-cracked Stage

The first stage occurs before the cracking shear load and is very similar for all specimens. It is characterized by a relatively linear relationship between the shear displacement and the applied shear load (Figure 4.2.a), negligible interface crack widths (Figure 4.2.c) and low interface steel reinforcement strains (Figure 4.2.e). The majority of the loading applied during the first stage is resisted by concrete shear associated with the strength of the bond between the two surfaces that form the shear interface.

4.2.2 Stage 2: Post Cracked Stage

The second stage occurs following cracking but before reaching the ultimate shear load. It is characterized by a softer overall response, larger and visible interface crack widths, and higher interface steel reinforcement strains than in the first stage. During the second stage both the shear displacements and crack widths exhibit a relatively linear relationship with the applied shear load, as can be seen in Figures 4.2.a and 4.2.c, respectively. The shear friction mechanism

starts to develop during the second stage after the strength of the concrete bond is no longer present. The capacity is primarily due to the friction that originates from the roughness of the two concrete surfaces that form the shear interface, which are tied together by the interface steel reinforcement. Because of the still low interface steel reinforcing strains (Figure 4.2.e), there is little active clamping force across the interface in this stage.

4.2.3 Stage 3: Post Ultimate Load Stage

The third stage occurs after the ultimate shear load of the specimens has been achieved. This stage is characterized by an increase in shear displacements, crack widths and interface steel reinforcement strains without any additional increase in applied loading. However, as seen in Figure 4.2, the behavior of the specimens with ASTM A615 interface steel reinforcement in this stage is different than that of the specimens with ASTM A1035 steel reinforcement. The specimens with ASTM A1035 steel reinforcement exhibit continued load carrying capacity after the ultimate shear load is achieved, which can be seen as a plateau in the load-displacement (V-Δ), load-crack width (V-w) and load-interface steel reinforcement strain (V-ε_s) plots shown in Figure 4.2. The specimens with ASTM A615 steel reinforcement, on the other hand demonstrate a more rapid degradation in post-ultimate load behavior. While this study is unable to determine the reasons for the different Stage 3 behavior, it is proposed that it may be due to the reportedly improved bond behavior of ASTM A1035 steel (Sumpter (2007) and Section 1.1.3) associated with its rib configuration. However, in the present study there was no discernable difference in rib configuration between the ASTM A615 and A1035 bars. This effect will be discussed further in Section 4.3.1.

4.3 ANALYSIS OF EXPERIMENTAL FINDINGS

In general, from the results of the push-off experiments summarized in Table 4.1 it can be seen that, as expected, the shear friction capacity of the specimens increased as the area of interface steel reinforcement increased. This is because the area of interface steel reinforcement is proportional to the clamping force (i.e. $F_s = f_s A_s$, where: $f_s = \varepsilon_s E_s$) and thus the shear friction capacity.

On the other hand, from the results in Table 4.1 it can be seen that the use of ASTM A1035 high-strength steel instead of ASTM A615 steel as interface reinforcement did not increase the shear friction capacity of the specimens significantly. This is because in all the specimens the ultimate shear load was reached well before steel yielding occurred. In fact, as seen in Table 3.2, the stress in the interface steel reinforcement is significantly lower than its yield strength when the ultimate shear load is achieved. The slight increase in capacity of the specimens with ASTM A1035 interface steel reinforcement may be attributed to the enhanced bond characteristics of this steel (Sumpter 2007), because a better bond results in higher steel strains and thus increases the shear friction capacity of the interface. This is discussed in the context of the present study in Section 4.3.1.

From Equations 4.1 through 4.4 it would be expected that the use of high-strength interface steel reinforcement would increase the shear friction capacity of the push-off specimens. In fact, if the interface steel reinforcement had reached its yield strength during the experiments it would be expected that specimens P-615-4 and P-1035-3, having similar nominal $A_{vf}f_y$ values, would have achieved similar shear friction capacities. This was not the case. In fact from Table 4.1 it can be seen that specimens P-615-4 had a significantly greater capacity than specimens P-1035-3, even though the latter had high-strength interface steel reinforcement.

These results show that the ASTM A1035 interface steel reinforcement does not increase the shear friction capacity significantly because the ultimate shear capacity is dominated by concrete behavior and is reached well before yielding occurs. Therefore, since the steel remains elastic, the clamping force is a function of the steel modulus, rather than the yield strength.

From the findings discussed in this section it can be inferred that Equations 4.1 through 4.4 do not represent correctly the shear friction phenomenon, since they assume that the interface steel reinforcement is yielding before or at the point that the ultimate shear load is reached. In addition, all the equations appear to oversimplify the real shear friction mechanism since the staged behavior, described in Section 4.2 is ignored. Nonetheless, it is noted that by empirically limiting the yield strength, f_y, to 60 ksi, these equations provide safe design values.

4.3.1 Apparent bond characteristics of A615 and A1035 bars

This study was not intended to investigate bond characteristics of the bars used, however the available crack opening versus interface steel strain data does allow a cursory evaluation of bond. Figure 4.3 shows representative interface steel reinforcement strain versus crack opening data from Specimens P-615-4A and P-1035-4A. It is noted that, consistent with the bond discussion, the steel strains in all cases are well below yield and thus the steel modulus controls behavior over the range shown.

All things being equal, once a crack occurs, the steel bridging that crack should have the same stress provided both the steel modulus and transfer of stress to the concrete through bond are the same. Clearly, the elastic moduli of A615 and A1035 bars are equivalent. Thus, the bond characteristics, and therefore the contribution of bond slip to the total crack opening must be different. Greater slip results in a lower bar stress for a given crack opening since the stress

transferred to the bar is only associated with the non-slip induced strain. This behavior is evident in Figure 4.3 in the post-peak behavior. Thus the results from the present study appear to support the assertion of Sumpter (2007) that the bond characteristics of A1035 bars is improved over that of A615 bars. Nonetheless, it is not appropriate to make this observation a generalization since different bar manufacturers will have different deformation patterns and therefore bond characteristics.

4.4 COMPARISON WITH PREVIOUS EXPERIMENTAL DATA

The relationship between the ultimate shear load, V_u, and the interface steel reinforcement area, A_{vf}, for the current experimental data is plotted in Figure 4.4. For comparison purposes, the plot also shows previous experimental data from shear friction tests performed by Hofbeck et al. (1969) and Kahn and Mitchell (2002) using monolithically cast uncracked (U), cold-jointed (CJ) and monolithically cast pre-cracked (C) specimens. Data points from previous experiments that were clearly outliers are not included in the plot. The data set is normalized with respect to the measured area of the concrete shear interface, A_{cv}, the measured concrete compressive strength, f'_c, and the elastic modulus, E_s, of the steel (E_s = 29,000 ksi). Note that the yield strength, f_y, of the interface steel reinforcement was not used to normalize the data because, as mentioned previously, the steel reinforcement does not reach its yield stress until after failure, thus the clamping force is a function of the elastic modulus rather than the yield strength of the steel.

From Figure 4.4 it can be seen that there is a significant difference between the normalized capacities of the uncracked, cold-jointed and pre-cracked specimens. In general the monolithically cast uncracked specimens have the greatest capacity, followed by the cold-jointed

specimens and then the pre-cracked specimens. This behavior is expected since monolithically cast specimens lack a defined shear interface. On the other hand, the cold-jointed specimens have a defined interface, which makes them weaker than the uncracked specimens. However the concrete bond between the two cast surfaces gives them more capacity than the pre-cracked specimens, which, although monolithically cast, are deliberately cracked prior to the push-off tests being conducted.

From Figure 4.4 it can also be seen that the data points from the current and previous experiments are consistent. However, the normalized capacity obtained with the current experiments, which were performed on cold-jointed specimens, is lower than the normalized capacity of the cold-jointed specimens tested by Kahn and Mitchell (2002). This difference can likely be attributed to the variation of the properties of concrete (Kahn and Mitchell tested high strength concrete specimens as shown in Table 1.5).

Finally, from Figure 4.4 it can be seen that the data set exhibits a relatively linear behavior until the normalized reinforcement ratio, $\rho_v E_s / f'_c$, is approximately 80. After this value the data set exhibits much greater scatter and starts to display a non-linear behavior. The reason for this change in behavior cannot be accurately established at this time. However it could just be a result of higher than normal reinforcement ratios ($\rho_v > 0.02$) on specimens with low concrete compressive strengths ($f'_c < 3500$ psi). In addition, it can be seen that after the normalized reinforcement ratio exceeds 80 the difference in capacity between the uncracked and pre-cracked specimens appears to become less significant; this may be artifact of the scatter of the results.

4.5 PROPOSED EQUATION

An equation to calculate the shear friction capacity of concrete members with cold-jointed (CJ) shear interfaces is derived from the plot in Figure 4.5. The approach to derive the equation is similar to that of Kahn and Mitchell (2002) with the difference that the elastic modulus of the interface steel reinforcement (E_s = 29,000 ksi) is used to normalize the data instead of its yield strength, f_y. Again, the reason for this is that the interface steel reinforcement does not reach its yield stress until after failure, thus the clamping force is a function of the elastic modulus of the steel rather than its yield strength. While this approach is still semi-empirical, it captures the actual behavior better than existing equations. Based on this approach, the proposed equation to calculate the shear friction capacity of concrete members with cold-jointed shear interfaces is:

$$V_{ni} = 0.060A_{cv}f'_c + 0.0014A_{vf}E_s \leq 0.2A_{cv}f'_c \qquad \text{(Eq. 4.5.a)}$$

The first term ($0.060A_{cv}f'_c$) of Equation 4.5.a represents the concrete component present during the first stage or pre-cracked stage of the shear friction mechanism as described in Section 4.2.1. This term, which is very similar to the one in Equation 4.4, defines in a conservative, yet accurate way, the value of the cracking shear load described in Section 3.1. The second term ($0.0014A_{vf}E$) of Equation 4.5.a represents the friction force generated by the interface steel reinforcement. The friction force starts to develop during the second stage or post cracked stage of the shear friction mechanism as described in Section 4.2.2 and increases until the ultimate shear load is reached. The friction force is the product of the clamping force, $\varepsilon_s A_{vf}E$, and coefficient of friction or friction factor, μ. In Equation 4.5.a the suggested 0.0014 factor is the product of the coefficient of friction or friction factor and the interface steel reinforcement strain at failure corresponding to a cold-joint interface with a surface condition of at least ¼-inch

amplitude. The value 0.0014 is in units of strain and reiterates the fact that the steel is not expected to yield since 0.0014 is less than the yield strain, ε_y, for steels having a yield strength, f_y, greater than 40 ksi. Finally, the limit of $0.2A_{cv}f'_c$ is kept equal to that proposed by Kahn and Mitchell (2002) since it agrees well with the experimental data.

A comparison between the observed and calculated cracking shear load ($0.060A_{cv}f'_c$), and the measured and calculated capacity for the current specimens is shown in Table 4.6. From Table 4.6 and Figure 4.5 it can be seen that Equation 4.5.a predicts in a conservative and accurate way the shear friction capacity of cold-jointed specimens. However, it underestimates and overestimates the capacity of monolithically cast uncracked (U) and pre-cracked (C) specimens, respectively. This is because, as mentioned previously, the uncracked specimens lack a defined shear interface, which increases the concrete component of the shear friction mechanism to a value higher than $0.060A_{cv}f'_c$, and the pre-cracked specimens are deliberately cracked prior to testing and therefore have a negligible concrete component. Therefore, for uncracked and pre-cracked concrete members the concrete component of the proposed equation needs to be calibrated against test data. Based on the limited test data available, the following modifications to Equation 4.5.a are proposed:

For uncracked members: $V_{ni} = 0.075A_{cv}f'_c + 0.0014A_{vf}E_s \leq 0.2A_{cv}f'_c$ (Eq. 4.5.b)

For pre-cracked members: $V_{ni} = 0.0014A_{vf}E_s \leq 0.2A_{cv}f'_c$ (Eq. 4.5.c)

The experimental results showed that the existing and previously proposed equations to calculate the shear friction capacity of concrete members underestimate the concrete component and overestimate the steel component of the shear friction mechanism. To address this problem, Equation 4.5 is calibrated using both the cracking and ultimate shear loads to better represent the stages of the shear friction mechanism, which results in a slightly higher concrete component

that is dependent on the concrete compressive strength, and a significantly lower steel component. This is illustrated in Figure 4.6, which shows a graphic comparison of the concrete and steel components of the shear friction capacity calculated with different equations for an arbitrary concrete member with concrete shear interface area, A_{cv}, equal to 160 in², shear interface steel reinforcement area, A_{vf}, equal to 1 in², and concrete compressive strength, f'_c, equal to 5 ksi.

Table 4.1: Summary of experimental results.

Specimen	A_{cv}, in² (mm²)	Interface Steel	A_{vf}, in² (mm²)	f_y, ksi (MPa)	V_{crack}, kips (kN)	Avg.	$\tau_{crack} = V_{crack}/A_{cv}$, ksi (MPa)	Avg.	V_u, kips (kN)	Avg.	$\tau_u = V_u/A_{cv}$, ksi (MPa)	Avg.
P-615-3A	160.4 (103484)	6 #3 A615	0.66 (426)	67.3 (464)	66.2 (294.5)	66.5 (295.8)	66.2 (294.5)	66.5 (295.8)	112.5 (500.2)	104.5 (464.7)	0.70 (4.8)	0.65 (4.5)
P-615-3B	163.2 (105290)	6 #3 A615	0.66 (426)	67.3 (464)	66.8 (297.1)		66.8 (297.1)		96.5 (429.2)		0.59 (4.1)	
P-615-4A	165.0 (106451)	6 #4 A615	1.20 (774)	61.5 (424)	50.0 (222.4)	54.1 (240.6)	50.0 (222.4)	54.1 (240.6)	114.5 (509.1)	121.7 (541.5)	0.69 (4.8)	0.74 (5.1)
P-615-4B	162.5 (104839)	6 #4 A615	1.20 (774)	61.5 (424)	58.2 (258.9)		58.2 (258.9)		129.0 (573.8)		0.79 (5.5)	
P-1035-3A	157.5 (101613)	6 #3 A1035	0.66 (426)	130.0 (896)	57.2 (254.6)	64.9 (288.6)	57.2 (254.6)	64.9 (288.6)	90.0 (400.3)	97.5 (433.7)	0.57 (3.9)	0.61 (4.2)
P-1035-3B	160.7 (103677)	6 #3 A1035	0.66 (426)	126.0 (869)	72.5 (322.6)		72.5 (322.6)		105.0 (467.0)		0.65 (4.5)	
P-1035-4A	162.5 (104839)	6 #4 A1035	1.20 (774)	140.0 (965)	58.4 (260.0)	59.2 (263.4)	58.4 (260.0)	59.2 (263.4)	135.7 (603.6)	124.6 (554.3)	0.84 (5.8)	0.77 (5.3)
P-1035-3B	160.7 (103677)	6 #4 A1035	1.20 (774)	131.3 (905)	60.0 (266.7)		60.0 (266.7)		113.5 (505.0)		0.71 (4.9)	

Table 4.2: AASHTO (Eq. 4.1) calculated capacity versus experimental capacity.

Specimen	V_u, kips (kN)	Avg.	f_y = 60 ksi (414 MPa) V_{ni}, kips (kN)	Avg.	V_u/V_{ni}	Avg.	Measured f_y V_{ni}, kips (kN)	Avg.	V_u/V_{ni}	Avg.
P615-3A	112.5 (500.2)	104.5 (464.7)	78.1 (347.4)	78.4 (348.9)	1.44	1.33	82.9 (368.8)	83.3 (370.3)	1.36	1.26
P615-3B	96.5 (429.2)		78.8 (350.4)		1.23		83.6 (371.8)		1.15	
P615-4A	114.5 (509.1)	121.7 (541.5)	111.3 (495.1)	111.3 (494.4)	1.03	1.09	113.1 (503.1)	113.1 (502.4)	1.01	1.08
P615-4B	129.0 (573.8)		111.0 (493.8)		1.16		112.8 (501.8)		1.14	
P1035-3A	90.0 (400.3)	97.5 (433.7)	77.4 (344.3)	77.8 (346.0)	1.16	1.25	122.7 (545.6)	122.7 (543.6)	0.73	0.80
P1035-3B	105.0 (467.0)		78.2 (347.7)		1.35		121.7 (541.5)		0.87	
P1035-4A	135.7 (603.6)	124.6 (554.3)	110.8 (492.8)	110.8 (492.3)	1.25	1.14	201.6 (896.6)	201.6 (884.5)	0.69	0.63
P1035-4B	113.5 (505.0)		110.6 (491.8)		1.03		196.1 (872.4)		0.58	

Table 4.3: ACI (Eq. 4.2) calculated capacity versus experimental capacity.

Specimen	V_u, kips (kN)	Avg.	f_y = 60 ksi (414 MPa)				Measured f_y			
			V_{ni}, kips (kN)	Avg.	V_u/V_{ni}	Avg.	V_{ni}, kips (kN)	Avg.	V_u/V_{ni}	Avg.
P615-3A	112.5 (500.2)	104.5 (464.7)	39.6 (176.1)	39.6 (176.1)	2.84	2.64	44.4 (197.6)	44.4 (197.6)	2.53	2.35
P615-3B	96.5 (429.2)		39.6 (176.1)		2.44		44.4 (197.6)		2.17	
P615-4A	114.5 (509.1)	121.7 (541.5)	72.0 (320.3)	72.0 (320.3)	1.59	1.69	73.8 (328.3)	73.8 (328.3)	1.55	1.65
P615-4B	129.0 (573.8)		72.0 (320.3)		1.79		73.8 (328.3)		1.75	
P1035-3A	90.0 (400.3)	97.5 (433.7)	39.6 (176.1)	39.6 (176.1)	2.27	2.47	84.5 (375.8)	84.5 (372.8)	1.06	1.17
P1035-3B	105.0 (467.0)		39.6 (176.1)		2.67		83.2 (369.9)		1.27	
P1035-4A	135.7 (603.6)	124.6 (554.3)	72.0 (320.3)	72.0 (320.3)	1.92	1.75	130.0 (578.3)	129.3 (575.1)	1.06	0.97
P1035-4B	113.5 (505.0)		72.0 (320.3)		1.58		128.6 (571.9)		0.88	

Table 4.4: Birkeland and Birkeland (Eq. 1.1) calculated capacity versus experimental capacity.

Specimen	V_u, kips (kN)	Avg.	f_y = 60 ksi (414 MPa)				Measured f_y			
			V_{ni}, kips (kN)	Avg.	V_u/V_{ni}	Avg.	V_{ni}, kips (kN)	Avg.	V_u/V_{ni}	Avg.
P615-3A	112.5 (500.2)	104.5 (464.7)	55.4 (246.6)	55.4 (246.6)	2.03	1.88	62.2 (276.6)	62.2 (276.6	1.81	1.68
P615-3B	96.5 (429.2)		55.4 (246.6)		1.74		62.2 (276.6)		1.55	
P615-4A	114.5 (509.1)	121.7 (541.5)	100.8 (448.4)	100.8 (448.4)	1.13	1.21	103.3 (459.6)	103.3 (459.6)	1.11	1.18
P615-4B	129.0 (573.8)		100.8 (448.4)		1.28		103.3 (459.6)		1.25	
P1035-3A	90.0 (400.3)	97.5 (433.7)	55.4 (246.6)	55.4 (246.6)	1.62	1.76	118.3 (526.1)	117.3 (522.0)	0.76	0.83
P1035-3B	105.0 (467.0)		55.4 (246.6)		1.91		116.4 (517.9)		0.91	
P1035-4A	135.7 (603.6)	124.6 (554.3)	100.8 (448.4)	100.8 (448.4)	1.37	1.25	130.0 (578.3)	129.3 (575.1)	1.06	0.97
P1035-4B	113.5 (505.0)		100.8 (448.4)		1.13		128.6 (571.9)		0.88	

Table 4.5: Kahn and Mitchell (Eq. 1.5) calculated capacity versus experimental capacity.

Specimen	V_u, kips (kN)	Avg.	f_y = 60 ksi (414 MPa)				Measured f_y			
			V_{ni}, kips (kN)	Avg.	V_u/V_{ni}	Avg.	V_{ni}, kips (kN)	Avg.	V_u/V_{ni}	Avg.
P615-3A	112.5 (500.2)	104.5 (464.7)	102.0 (453.5)	102.4 (455.3)	1.10	1.02	108.7 (483.5)	109.1 (485.3)	1.03	0.96
P615-3B	96.5 (429.2)		102.8 (457.1)		0.94		109.5 (487.1)		0.88	
P615-4A	114.5 (509.1)	121.7 (541.5)	148.7 (661.2)	148.3 (659.6)	0.77	0.82	151.2 (672.4)	150.8 (670.8)	0.76	0.81
P615-4B	129.0 (573.8)		147.9 (658.0)		0.87		150.4 (669.2)		0.86	
P1035-3A	90.0 (400.3)	97.5 (433.7)	101.1 (449.8)	101.6 (451.8)	0.89	0.96	165.8 (737.5)	164.4 (731.3)	0.54	0.60
P1035-3B	105.0 (467.0)		102.0 (453.9)		1.04		163.0 (725.2)		0.65	
P1035-4A	135.7 (603.6)	124.6 (554.3)	147.9 (658.0)	147.7 (656.8)	0.93	0.85	188.5 (838.5)	187.5 (833.8)	0.73	0.67
P1035-4B	113.5 (505.0)		147.4 (655.7)		0.77		186.4 (829.2)		0.61	

Table 4.6: Calculated versus experimental capacity using proposed equation (Eq. 4.5.a).

Specimen	V_{crack}, kips (kN)	$0.06A_{cv}f'_c$, kips (kN)	$V_{crack}/0.060A_{cv}f'_c$	V_u, kips (kN)	$V_{ni} = 0.060A_{cv}f'_c + 0.0014A_{vf}E$, kips (kN)	V_u/V_{ni}
P615-3A	66.2 (294.5)	55.8 (248.3)	1.2	112.5 (500.2)	82.6 (367.4)	1.4
P615-3B	66.8 (297.1)	56.8 (252.6)	1.2	96.5 (429.2)	83.6 (371.8)	1.2
P615-4A	50.0 (222.4)	57.4 (255.4)	0.9	114.5 (509.1)	106.1 (472.1)	1.1
P615-4B	58.2 (258.9)	56.5 (54.8)	1.0	129.0 (573.8)	105.3 (468.2)	1.2
P1035-3A	57.2 (254.6)	54.8 (243.8)	1.0	90.0 (400.3)	81.6 (363.0)	1.1
P1035-3B	72.5 (322.6)	55.9 (248.7)	1.3	105.0 (467.0)	82.7 (367.9)	1.3
P1035-4A	58.4 (260.0)	56.5 (251.5)	1.0	135.7 (603.6)	105.3 (468.2)	1.3
P1035-4B	60.0 (266.7)	55.9 (248.7)	1.1	113.5 (505.0)	104.6 (465.4)	1.1

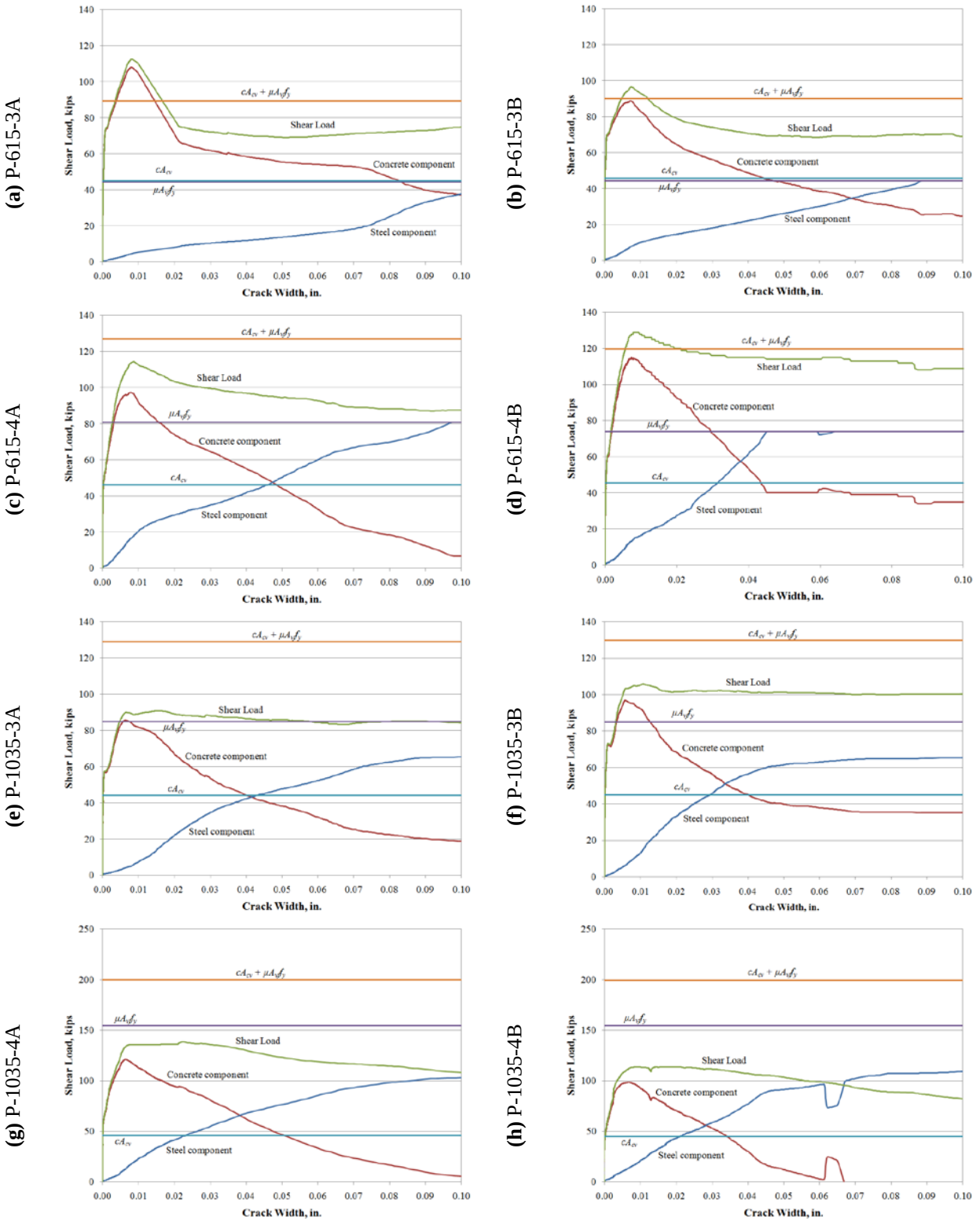

Figure 4.1: Shear friction behavior as described by AASHTO (using measured f_y).

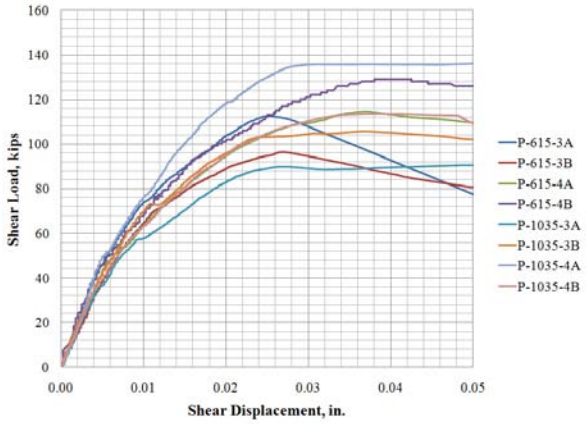

(a) Shear load versus average shear displacement

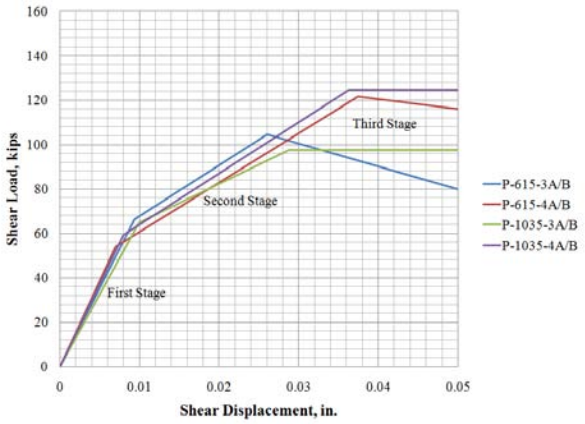

(b) Linearization of shear load versus average shear displacement showing described stages of the shear friction mechanism.

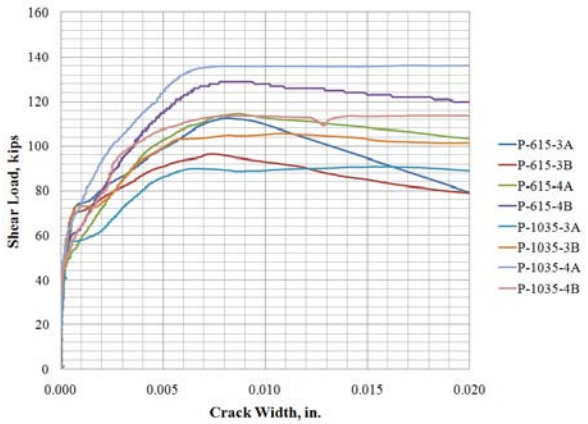

(c) Shear load versus average crack width

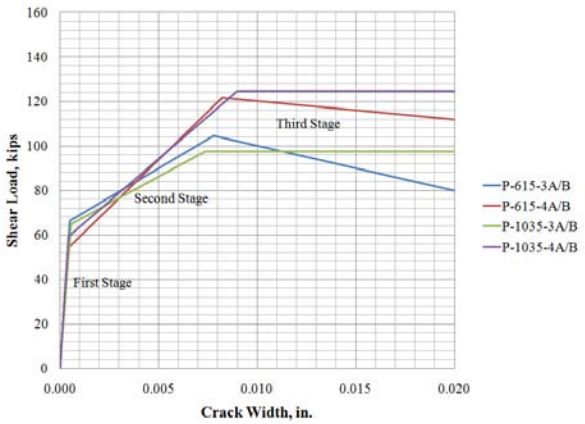

(d) Linearization of shear load versus average crack width showing described stages of the shear friction mechanism.

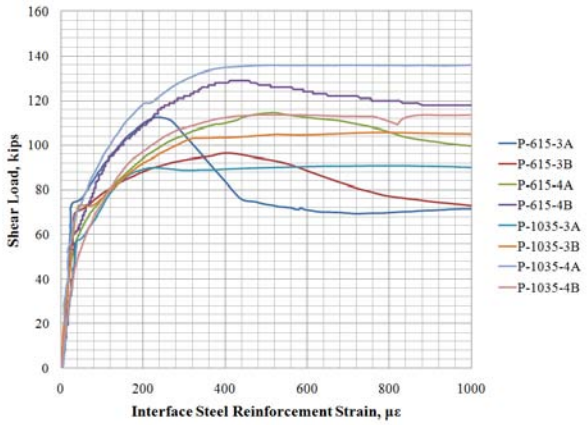

(e) Shear load versus average interface steel strain

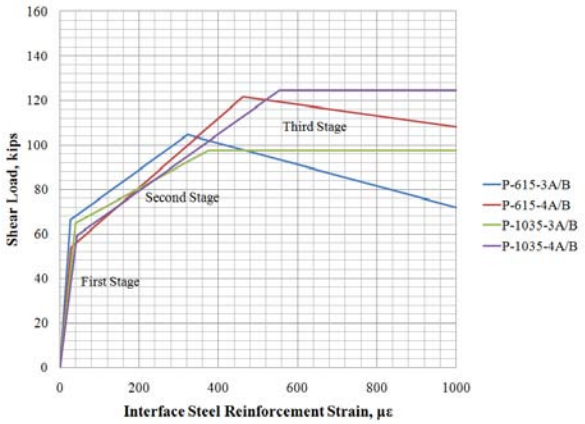

(f) Linearization of shear load versus average interface steel strain showing described stages of the shear friction mechanism.

Figure 4.2: Comparison and linearization of test results for each specimen.

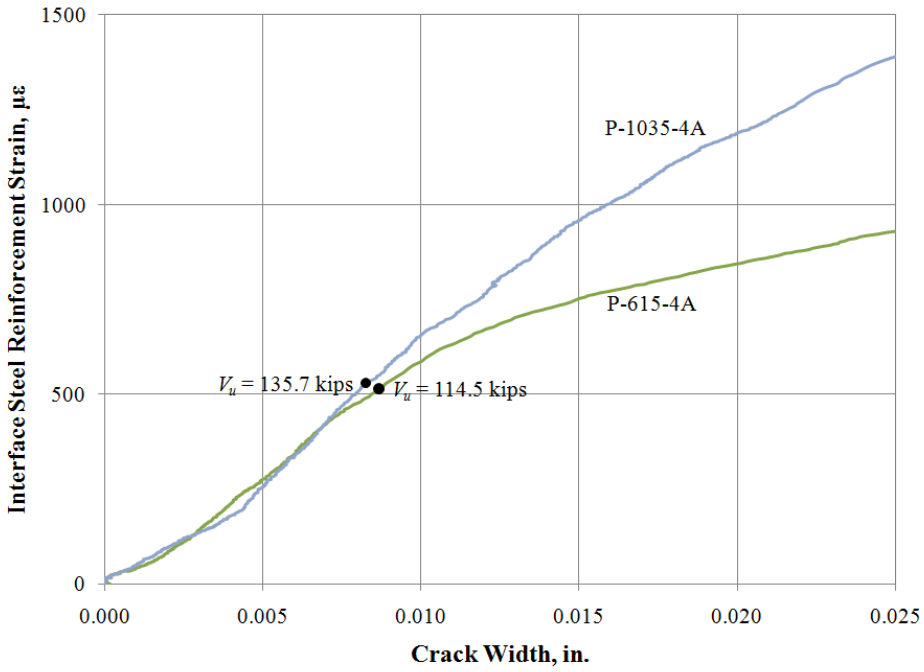

Figure 4.3: Representative plots of interface steel reinforcement strain versus crack opening.

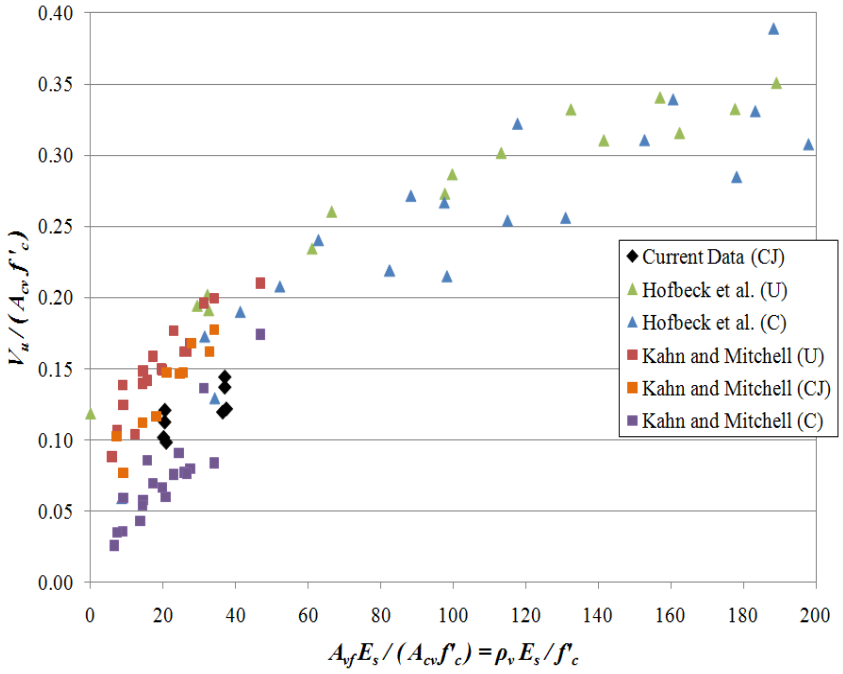

Figure 4.4: Normalized experimental data from current and previous experiments.

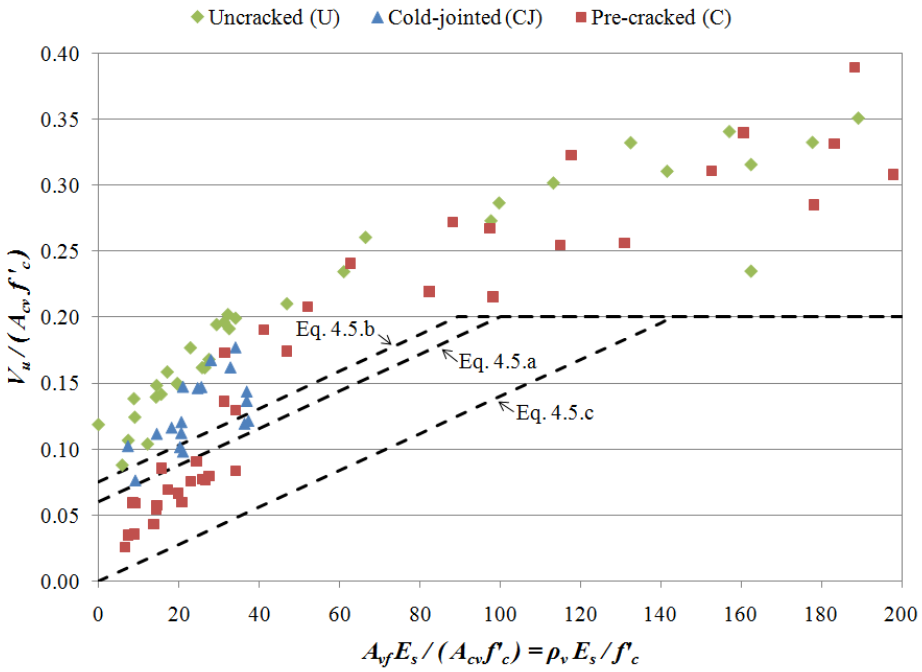

Figure 4.5: Proposed shear friction equation.

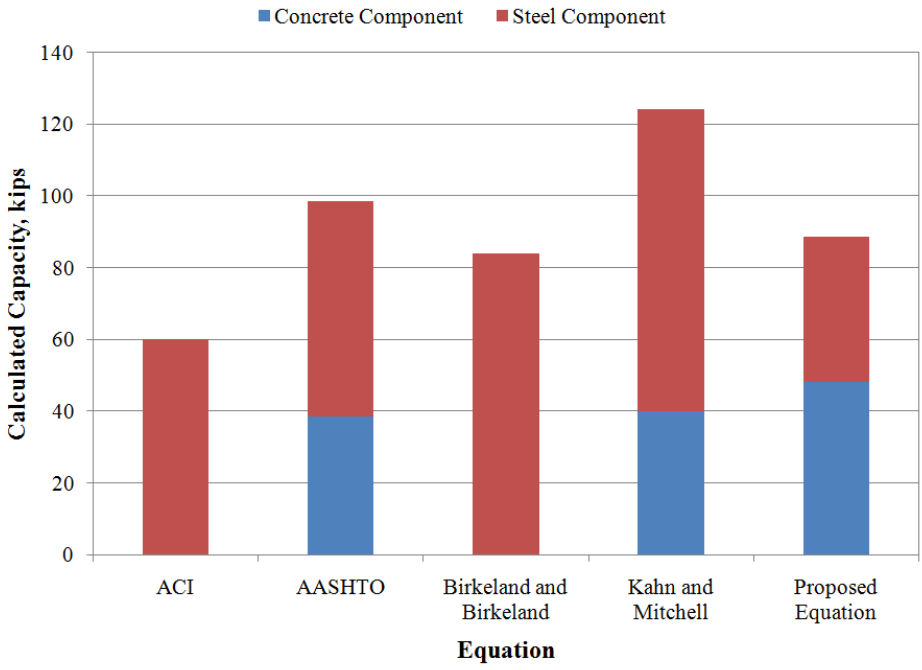

Figure 4.6: Comparison of concrete and steel components of shear friction mechanism.

5.0 CONCLUSIONS

The objective of the study was to evaluate the effects of the use of high-strength steel reinforcement in shear friction applications. The study was accomplished by testing typical push-off specimens with a cold joint test interface, which had a surface condition with at least ¼-inch amplitude in order to simulate the connection between a composite slab and an AASHTO girder. The interface steel reinforcement consisted of either ASTM A615 or ASTM A1035 bars.

The test results showed that the shear friction mechanism occurs in stages and that the concrete component contributes to the majority of the shear friction capacity prior to cracking when the steel component develops. In other words, the concrete and steel components of the shear friction mechanism do not act simultaneously as implied by the present AASHTO shear friction equation (Eq. 4.1). In addition, the test results showed that, contrary to the assumptions of the AASHTO and ACI equations to calculate the shear friction capacity of concrete members, the interface steel reinforcement never reaches its yield strain. Therefore, the use of high-strength reinforcing steel does not affect the shear friction capacity of concrete members because the clamping force is a function of the elastic modulus of the steel rather than its yield strength.

Based on these findings and using the experimental data from current and previous tests, Equation 4.5 was proposed as an alternative to the existing AASHTO and ACI equations to calculate the shear friction capacity of concrete members. While the proposed equation is still semi-empirical, it represents the actual shear friction behavior better than the existing equations

because it is calibrated using both the cracking and ultimate shear loads to better represent the stages of the shear friction mechanism, which results in a slightly higher concrete component that is dependent on the concrete compressive strength, and a significantly lower steel component than those predicted with the existing equations. In addition, the proposed equation is a function of the elastic modulus of steel rather than its yield strength based on the experimental results, which showed that the interface steel reinforcement does not reach its yield strain until after failure of the specimens.

Despite the foregoing discussion, the existing empirical ACI and AASHTO equations for shear friction capacity are appropriate for design provided the value of the yield strength, f_y, is not taken greater than 60 ksi as is currently the AASHTO recommendation.

5.1 RECOMMENDATIONS FOR FUTURE RESEARCH

The proposed equation (Equation 4.5) to calculate the shear friction capacity of concrete members is based on limited data obtained from current and previous shear friction experiments. In order to verify the accuracy of the factors in the proposed equation, as well as to calibrate it for different parameters the following actions are recommended for future research:

- Increase the number of specimens tested in order to have a more significant statistical sample size.
- Test specimens with different shear interface types (uncracked, cold-jointed, pre-cracked) and surface conditions to obtain different calibration factors for the concrete and steel components of the proposed equation.

- Test specimens with different interface steel reinforcement areas, A_{vf}, to verify that the reinforcement ratio, ρ_v, is linearly proportional to the shear friction capacity and to what extent.
- Test specimens with different concrete compressive strength, f'_c, to determine if the calibrating factor for the concrete component of the proposed equation is accurate.

BIBLIOGRAPHY

ACI Committee 318. Building Code Requirements for Structural Concrete (ACI 318-08) and Commentary (ACI 318R-08). Farmington Hills, MI: American Concrete Institute, 2008.

American Association of State Highway and Transportation Officials (AASHTO). AASHTO LRFD Bridge Design Specifications. 4th edition. 2007.

ASTM A1035/A1035M-07. Standard Specification for Deformed and Plain, Low-Carbon, Chromium, Steel Bars for Concrete Reinforcement. Conshohocken, PA: ASTM International, 2007.

ASTM A615/A615M-06. Standard Specification for Deformed and Plain Carbon-Steel for Concrete Reinforcement. Conshohocken, PA: ASTM International, 2006.

ASTM C192/C192M-06. Standard Practice for Making and Curing Concrete Test Specimens in the Laboratory. ASTM International, 2006.

ASTM C39/C39M-05e1. Standard Test Method for Compressive Strength of Cylindrical Concrete Specimens. ASTM International, 2005.

Birkeland, P. W., and H. W. Birkeland. "Connections in Precast Concrete Construction." Journal of the American Concrete Institute 63, no. 3 (1966): 345-368.

Hanson, N. W. "Precast-Prestressed Concrte Bridges - 2. Horizontal Shear Connections." Journal PCA Research and Development Laboratories 2, no. 2 (1960): 38-58.

Hassan, T. K., H. M. Seliem, H. Dwairi, S. H. Rizkalla, and P. Zia. "Shear Behavior of Large Concrete Beams Reinforced with High-Strength Steel." ACI Structural Journal 105, no. 2 (2008): 173-179.

Hofbeck, J. A., I. O. Ibrahim, and A. H. Mattock. "Shear Transfer in Reinforced Concrete." Journal of the American Concrete Institute 66, no. 2 (1969): 119-128.

Kahn, L. F., and A. D. Mitchell. "Shear Friction Tests with High Strength Concrete." ACI Structural Journal 99, no. 1 (2002): 98-103.

Lepage, A., H. Tavallali, S. Pujol, and J. Rautenberg. "Towards Earthquake-Resistant Concrete Structures with Ultra High-Strength Steel Reinforcement." 14th World Conference on Earthquake Engineering. Beijing: International Association for Earthquake Engineering, 2008.

Loov, R. E., and A. K. Patnaik. "Horizontal Shear Strength of Composite Concrete Beams with a Rough Interface." PCI Journal 39, no. 1 (1994): 48-69.

Mast, R. F., M. Dawood, S. M. Rizkalla, and P. Zia. "Flexural Strength Design of Concrete Beams Reinforced with High-Strength Steel Bars." ACI Structural Journal 105, no. 4 (2008): 570-577.

Mattock, A. H. "Shear Transfer in Concrete Having Reinforcement at an Angle to the Shear Plane." ACI Special Publication 42 - Shear in Reinforced Concrete, 1974: 17-42.

Nawy, E. G. "Crack control in reinforced concrete structures." ACI Structural Journal 65, no. 10 (1968): 825-836.

Rizkalla, S., R. El-Hacha, and H. Elagroudy. "Bond Characteristics of High-Strength Steel Reinforcement." ACI Structural Journal 103, no. 6 (2006): 771-782.

Seliem, H. M., G. Lucier, S. H. Rizkalla, and P. Zia. "Behavior of Concrete Bridge Decks Reinforced with High-Performance Steel." ACI Structural Journal 105, no. 1 (2008): 78-86.

Shahrooz, B. M., Harries, K. A., Miller R., and Russell, H. "NCHRP Project 12-77 Interim and Quarterly reports." 2006-2009.

Sumpter, M. S. "Behavior of High Performance Steel as Shear Reinforcement for Concrete Beams." ACI Structural Journal 106, no. 2 (2007): 171-177.

Walraven, J. C., and H. W. Reinhardt. "Theory and Experiments on the Mechanical Behaviour of Cracks in Plain and Reinforced Concrete Subject to Shear Loading." Heron 26, no. 1A (1981): 68.

Walraven, J. C., J. Frenay, and A. Pruijssers. "Influence of Concrete Strength and Load History on the Shear Friction Capacity of Concrete Members." PCI Journal 32, no. 1 (1987): 66-84.